Thin-Walled Structures 170 (2022) 108596

Contents lists available at ScienceDirect

Thin-Walled Structures

journal homepage: www.elsevier.com/locate/tws

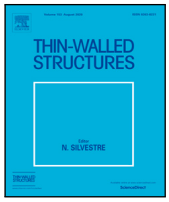

Full length article

Stress and buckling resistance of dual-purpose concrete shells

Alphose Zingoni

Department of Civil Engineering, University of Cape Town, Rondebosch 7701, Cape Town, South Africa

ARTICLE INFO

Keywords:
Dual-purpose shell
Thin concrete shell
Shell structure
Shell roof
Shell analysis
Shell stresses
Shell design
Shell buckling

ABSTRACT

In this contribution, and as an extension of previous work, the simultaneous use of thin concrete shells for roofing and liquid containment is explored, with a particular focus on the bending and buckling behaviour of the shell. The concept of dual-purpose concrete shells is a novel one, and has the potential to revive the widespread use of elegant thin concrete shells once again. It is shown how excessive stresses due to water loading can be controlled through gradual thickening of the shell over the submerged region. Not only are membrane stresses lowered, but the bending stresses in the vicinity of the shell edge are also significantly moderated. Through a linear eigenvalue buckling analysis followed by a nonlinear Riks-type buckling analysis accounting for geometric imperfections, such thickening is also shown to be effective in enhancing the buckling resistance of the shell. The overall conclusion is that the concept of dual-purpose concrete shells is structurally viable, and deserves more attention.

1. Introduction

Thin concrete shell roofs, once popular [1], have declined in their use, mainly as a result of the high costs of formwork for curved surfaces. The development of pneumatic formwork systems lowered costs quite significantly, and partially revived the use of thin concrete shell roofs, but overall construction costs still remained relatively high. Advances in fabric formwork [2–4] and form-finding techniques [5,6] have extended the possibilities for concrete shells as well as shells in other materials. While all these innovations have been very significant strides in the right direction, it is clear that if thin concrete shells are to regain their position in mainstream architecture and structural engineering, more needs to be done to allow greater benefit to be derived from the shell [7].

The superior structural efficiency of thin concrete shells stems from their ability to resist transverse surface loads predominantly by membrane action as opposed to bending which in turn, as Calladine explains [8,9], stems from the properties of "*surface*" and "*curvature*" that characterise their geometry. The curvature of the shell midsurface has a significant influence on the pattern of stresses within the shell [8]. Useful in understanding the response of the shell is the notion of Gaussian curvature, which is the product of the principal radii of curvature at any given point on the shell. Thus spherical domes and elliptic paraboloids, on account of their positive Gaussian curvature, respond differently to surface loads when compared with shells of negative Gaussian curvature such as hyperbolic paraboloids [10].

For membrane action to prevail in the shell, the shell has to fulfil certain smoothness conditions of geometry, material stiffness and loading, and also has to be supported in such a way that no bending moments occur at the edge of the shell [11,12]. Furthermore, concentrated loads on the shell must be avoided. If there are discontinuities in the shell, or if the shell is not supported in accordance with the assumptions of the membrane hypothesis, then significant bending may occur in the shell. Like most structural elements with finite rigidity, a shell is not as efficient when resisting transverse applied loads through bending as opposed to in-plane or extensional action, so as much as possible, bending must be avoided. In practice, even if interior smoothness conditions are met, bending effects can never be totally eliminated; good design becomes a matter of minimising flexural effects in the shell.

In evaluating the structural feasibility of new applications for thin shells in concrete, stress and buckling resistance rank among the most important considerations. One or more of three common approaches may be adopted. The analytical approach can provide useful insights on structural behaviour, and is well-suited to parametric study [12], but suffers the disadvantage of not being able to deal with complex or arbitrary problems. On the other hand, the numerical approach (such as finite-element modelling), while not amenable to the same level of parametric control as analytical solutions, is more versatile in handling complex situations, and is particularly useful in the evaluation of buckling behaviour and non-linear effects. The third approach, experimental testing, tends to be the most expensive, and has to be very specific in scope owing to the costs involved, but it is often the only reliable means of validating theoretical and numerical formulations. Here, we will only be concerned with the first two approaches.

The analytical approach is most effective for stress studies involving small elastic deformations [13], and where the geometry of the shell

E-mail address: alphose.zingoni@uct.ac.za.

https://doi.org/10.1016/j.tws.2021.108596
Received 3 July 2021; Received in revised form 10 October 2021; Accepted 22 October 2021
Available online 16 November 2021

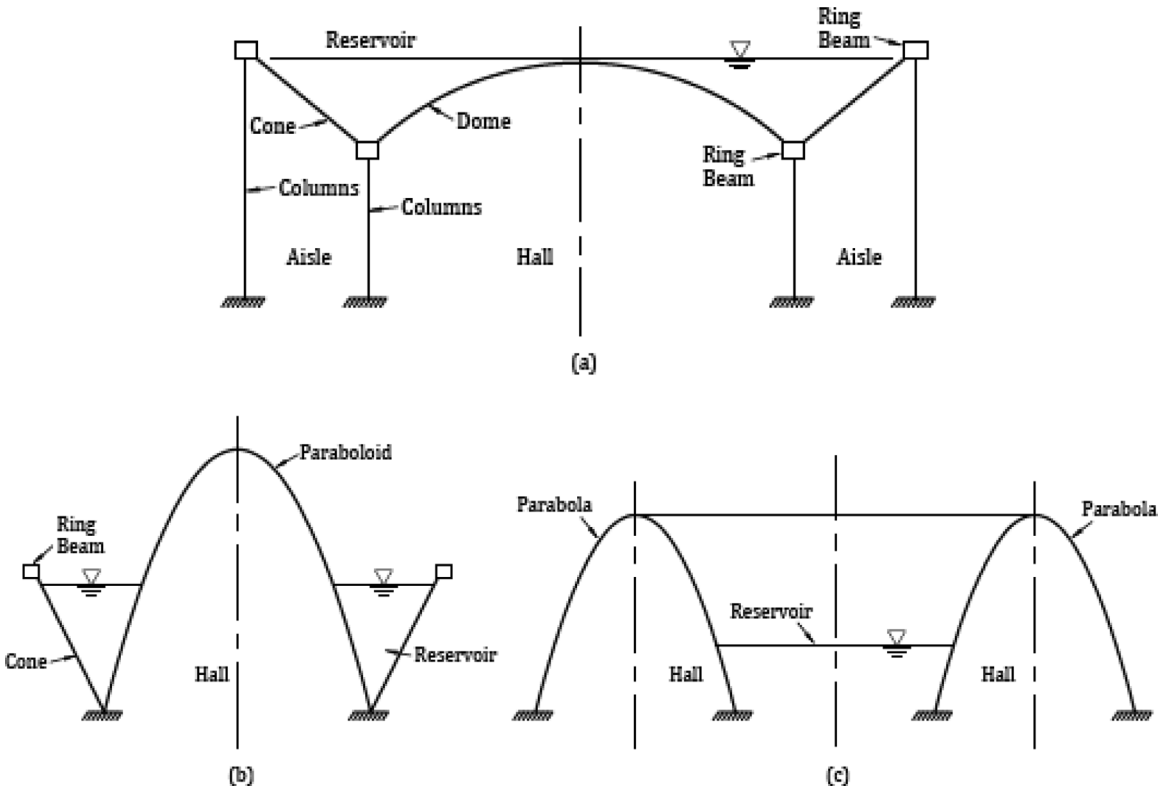

Fig. 1. Some dual-purpose concrete shells: (a) conical-spherical shell assembly serving as the roof of a large circular hall and the sloping walls and concave floor of an elevated water reservoir; (b) tall paraboloidal exhibition hall surrounded by a conical reservoir; (c) toroidal hall of parabolic cross-section with a central water reservoir.

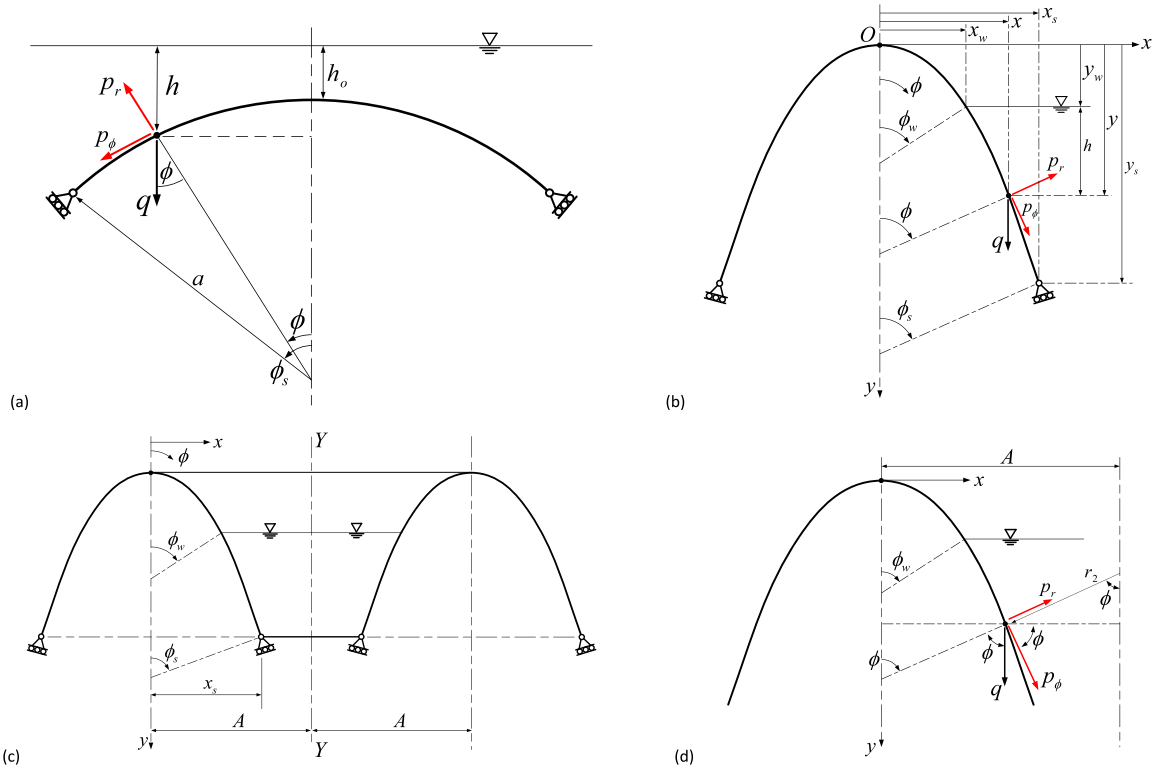

Fig. 2. Geometric and loading parameters of shells: (a) spherical dome; (b) paraboloid of revolution; (c) parabolic toroid: full cross-section; (d) parabolic toroid: left side of cross-section showing details.

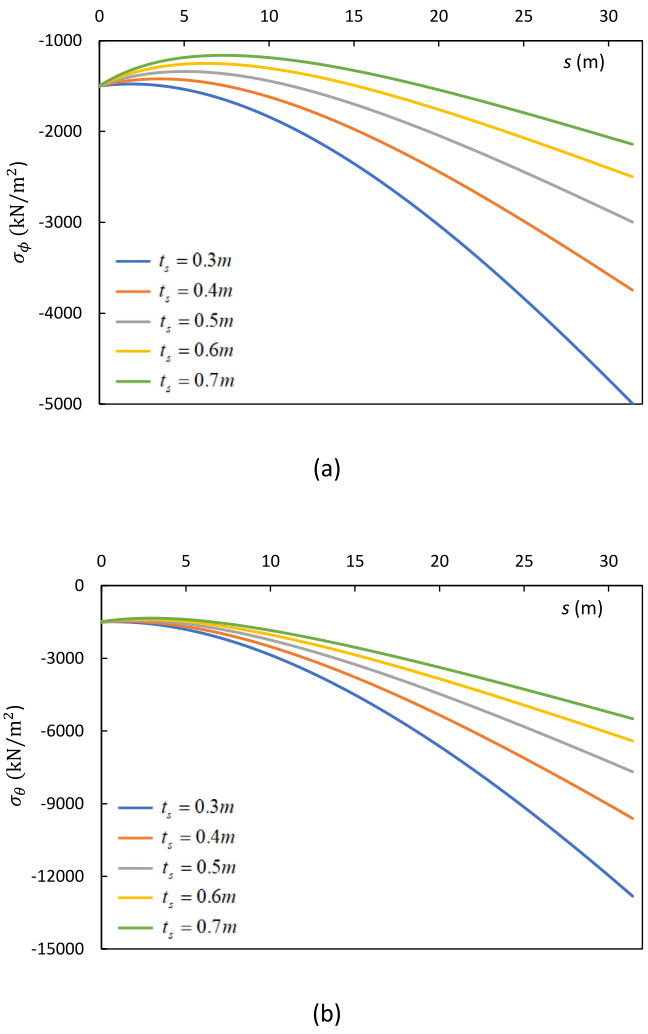

Fig. 3. Spherical dome: Variation of membrane stresses with arc length s for various degrees of shell thickening: (a) σ_ϕ variation; (b) σ_θ variation [7].

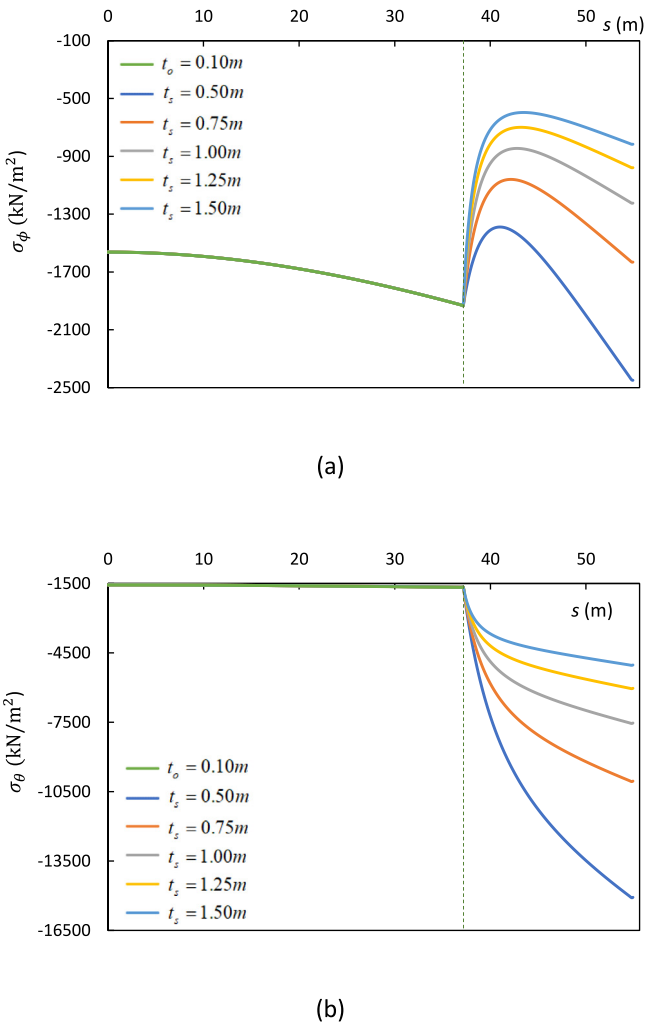

Fig. 4. Paraboloid of revolution: Variation of membrane stresses with arc length s for various degrees of shell thickening: (a) σ_ϕ variation; (b) σ_θ variation [7].

is relatively simple. The bending theory of shells (inclusive of the membrane theory) has been used to study stresses in spherical concrete domes [14], and to develop recommendations for design. The same theory has been used in studying discontinuity problems in liquid-containment shell structures, including spherical tanks [15], conical vessels [16], ellipsoids of revolution [17], elliptic toroids [18], and multi-shell vessels [19,20]. The much simpler membrane theory has also been successfully used on its own to evaluate the state of stress in a variety of shell structures, such as elliptic toroidal domes [21], cooling towers [22] and liquid-containment shells of unusual shape [23,24].

The buckling behaviour of shells subjected to external pressure has been extensively studied, with the majority of the studies having involved shells of zero Gaussian curvature (cylindrical and conical shells) [25,26]. Some studies have concentrated on theoretical aspects, examples being an investigation on long-term effects in shallow concrete domes [27], and a study on the buckling of complete spherical shells [28]. The elastic buckling of composite cylindrical shells under hydrostatic pressure has also been the subject of a very recent study [29]. As part of a programme of investigation on new possibilities for underwater observatories, the buckling behaviour of spherical-conical and spherical-paraboloidal assemblies under external hydrostatic pressure has also been studied [30]. Also featured in the literature have been studies of toroidal shells under uniform external pressure [31] and hydrostatic water pressure [32]. Interest in the toroidal geometry continues, as alternative cross-sectional profiles are explored [33,34]. From a loading point of view, buckling of shells under wind effects pose particularly challenging problems [35,36], while from a geometry point of view, the need to understand the behaviour of shells of unusual shape is an important part of the process of exploring and discovering more efficient shell forms for fluid containment [37,38].

We have noted the decline in the use of thin concrete shells for roofing over the years, and some of the developments that have been directed towards overcoming the challenges. To provide greater justification for the often-cited high costs of construction of thin concrete shell roofs, the author has recently proposed the dual use of concrete shells [7]. Usually a shell has one specific function, such as to provide roofing, or to retain liquid, but not both. To allow more benefit to be derived from the thin concrete shell, it has been proposed to utilise the same shell (in whole or in part) for two different functions: (i) as the curved roof (or full enclosure) of a circular hall, and (ii) as the curved floor (or curved retaining wall) of a water reservoir. Besides the dual use of the shell, these possibilities also promise a more efficient utilisation of urban land (the ground space that is normally occupied by a water reservoir is freed up for other purposes), and opportunities for significant energy savings.

In fact, the concept could be extended to multi-purpose shells. In hot climates, the cooling effect of the reservoir water on one side of the shell wall could allow users of the building to do away with the need for air-conditioning in the inhabited space on the other side. In semi-arid

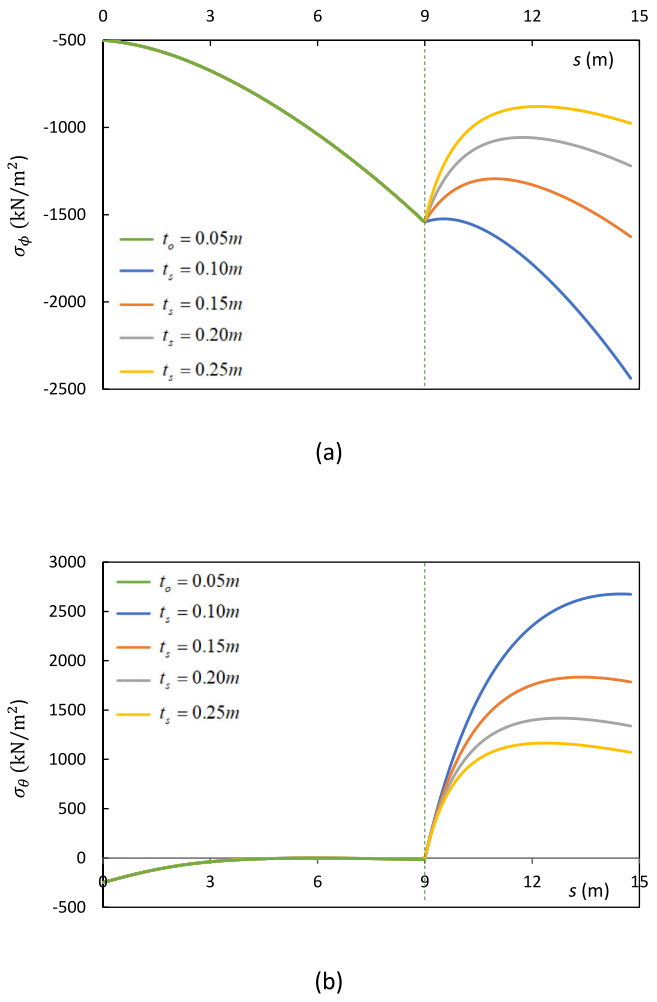

Fig. 5. Parabolic toroid: Variation of membrane stresses with arc length s for various degrees of shell thickening: (a) σ_ϕ variation; (b) σ_θ variation [7].

areas of the world which are prone to drought, rain water could be harvested from the curved surface of a shell roof, and directly stored in a reservoir that uses the same shell roof as a floor. A flat retractable cover could be installed over the reservoir to reduce evaporation. Solar panels could be mounted on such a cover to collect solar energy, making the shell structure effectively multi-purpose. Designing shell structures with energy savings in mind, or facilitating the use of renewable energy, is in keeping with the philosophy of sustainable engineering. Multi-purpose concrete shells hold promise of significantly adding value to the shell structure, and offsetting the high costs associated with the construction of curved surfaces, thereby helping to revive the use of thin concrete shells once again. A related concept has been the possible use of deployable hyperbolic-paraboloidal umbrella shells in coastal locations [39,40], where they can provide shelter from the sun or the rain under normal weather conditions, and can be deployed to act as flood barriers against sea waves during extreme weather conditions.

The novelty of the present work is not in proposing a new theory of shells nor a new numerical formulation for shells, but in exploring the use of thin concrete shell for dual use. In this paper, and as part of an ongoing programme of investigation, we will consider some possible configurations for dual-purpose concrete shells. The loadings of interest are the self-weight of the shell and the hydrostatic pressure of the water. In a previous study [7], the feasibility of dual-purpose concrete shells (spherical, conical, paraboloidal and parabolic-toroidal) was considered on the basis of the magnitude and distribution of membrane stresses in the shell, and gradual shell thickening was proposed over the submerged part of the shell, as a means for controlling the relatively high stresses that are induced by the water loading.

For three of the shells previously considered, the present paper extends the study of stresses to take into account the bending of the shell that occurs in the vicinity of the support, and the buckling that may occur in the lower regions of the shell. While an analytical approach is adopted for the estimation of bending-related stresses, finite-element modelling will be employed in the buckling investigation. Results for critical buckling pressures and mode shapes, derived from a linear eigenvalue FEM analysis, will be presented. A nonlinear buckling analysis accounting for imperfections, and tracing the post-buckling behaviour of the shell, will also be conducted. Hydrodynamic effects due to the sloshing of water do not form part of the present study.

2. Some dual-purpose concrete shells

There is no limit on the shell geometries that can be combined into a dual-purpose system. Dual-purpose concrete shells can take the form of shells of revolution, shells of translation, or some other class of shells. Here, we will focus on configurations in which the components of the system are shells of revolution, and the whole system has a central axis of rotation. Thus, the theory of shells of revolution may be used in the stress analysis. Fig. 1 shows three types of dual-purpose concrete shells. These will form the subject of the present study.

Fig. 1(a) shows a cross-section of a building whose roof system comprises a dual-purpose concrete dome and a dual-purpose conical-shell roof. The circular dome serves as the roof of a large circular hall, which could be a theatre, a place of worship or some other public facility. The conical frustum serves as the sloping roof of a circular aisle that runs around the circumference of the hall. The space above the two shells, bound between the inner surface of the conical shell and the outer surface of the circular dome, serves as a shallow water reservoir. This arrangement is an example of situations where the shell roof can be used for harvesting rain water (in those areas of the world which suffer from a scarcity of water), and storing the water in the shallow reservoir that is formed by the walls of the same shells.

The two-shell roof system is supported on two sets of vertical columns. The inner set of columns is located at the junction of the two shells. The outer set of columns is located at the upper edge of the conical shell. Ring beams provided at the top of the columns serve to distribute the reactions from the columns, and to absorb any horizontal thrust or pull exerted by the shells at their edges. Thus, the presence of a ring beam at the edge of a shell mitigates bending effects in the shell. In the configuration of Fig. 1(a), it should also be pointed out that the angle of inclination of the conical shell may be chosen in such a way that the horizontal thrust of the spherical dome upon the ring beam exactly balances the horizontal thrust of the conical shell, which then minimises the size of the required ring beam, hence the overall cost of the support system. The design of the support system lies outside the scope of this study.

Fig. 1(b) shows a paraboloid of revolution that is connected to a conical shell at the base, with the lower region of the paraboloid being surrounded by the walls of the conical shell. The inner paraboloidal space serves as an exhibition hall for tall equipment, while the outer space (bound between the outer surface of the paraboloid of revolution and the inner surface of the conical shell) serves as an elevated annular reservoir. In this configuration, the wall of the conical shell only serves the purpose of retaining the water, and therefore the conical shell is not a dual-purpose shell. On the other hand, the lower part of the paraboloid of revolution serves not only as the sides of the interior hall, but also as the inner wall of the water reservoir. Therefore, the paraboloid of revolution is a dual-purpose shell. To avoid perforating through the water reservoir, access into the hall may be provided via walkways located below the level of the shell supports, with stairs leading up onto the exhibition floor, or walkways located just above

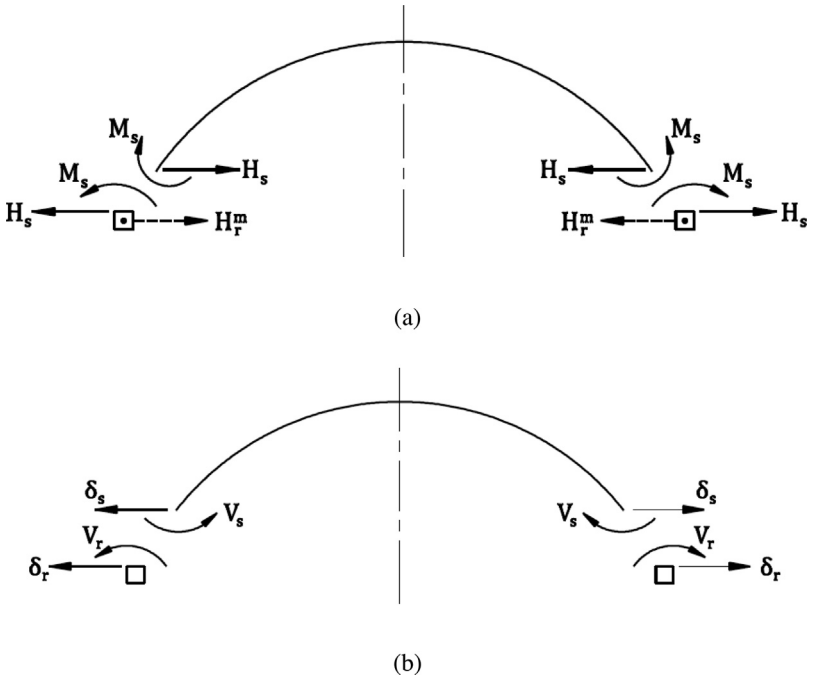

Fig. 6. Positive conventions for deformations and redundants at the edge of a shell. Where an edge beam is provided, the reactions on the edge beam are also shown.

the reservoir (footbridges), with stairs leading down onto the exhibition floor.

Fig. 1(c) shows a dual-purpose parabolic toroidal dome. A parabolic toroid is a surface of revolution that has the topology of a torus, except that the cross-section is an open parabola instead of a closed circle. The interior of the cross-section serves as a ring-shaped exhibition hall. The central open space of the toroid, which lies outside the cross-section of the toroid and faces the open sky, serves as a circular water reservoir. The anticlastic region of the toroidal shell (i.e. the inner region of negative Gaussian curvature) serves a dual purpose: it is the inner wall of the exhibition hall, and the retaining wall of the central water reservoir. The synclastic region of the toroidal shell (i.e. the outer region of positive Gaussian curvature) only serves as the outer wall of the exhibition hall, and therefore is not a dual-purpose region. For the purposes of this study, we will consider only the inner region of the parabolic toroidal dome that serves a dual purpose.

3. Membrane stresses

It is usual to adopt an angular coordinate system $\{\phi, \theta\}$ to describe the position of points on the midsurface of the shell [12,13], although for some geometries, a Cartesian coordinate system may be more convenient. With the axis of revolution of the shell taken to be vertical, and hoop circles taken to lie in horizontal planes, the vertical angle ϕ is the meridional angle, measured downward from the upward direction of the axis of revolution of the shell, to the normal to the shell midsurface at the point in question. The horizontal angle θ is the circumferential angle, measured from an arbitrary reference meridional plane, to the meridional plane in question.

For shells of revolution subjected to axisymmetric loading, only two stress resultants are relevant in a membrane analysis: N_ϕ^m (the meridional stress resultant) and N_θ^m (the hoop stress resultant), which are direct forces per unit length. We will consider N_ϕ^m and N_θ^m as positive if they are tensile, and as negative if they are compressive. Equilibrium considerations of a shell element subjected to these stress resultants and the applied loads (acting over the surface of the element) yield the well-known general solutions [12,13]:

$$N_\phi^m = \frac{1}{r_2 \sin^2\phi} \int \left\{ r_1 r_2 \left(p_r \cos\phi - p_\phi \sin\phi \right) \sin\phi \right\} \, d\phi + \beta \tag{1a}$$

$$N_\theta^m = r_2 p_r - \frac{r_2}{r_1} N_\phi^m \tag{1b}$$

In these expressions, r_1 and r_2 are the principal radii of curvature of the shell midsurface at the point in question; the parameters p_r and p_ϕ represent loading components expressed as forces per unit area of the shell surface (p_r in the direction of the normal to the shell midsurface, and p_ϕ in the direction of the tangent to the shell meridian); β is a constant of integration to be evaluated from a suitable boundary condition of the shell. Eqs. (1) are, of course, also applicable to conical shells, if r_1 is set equal to infinity and the angular coordinate ϕ is replaced with the distance coordinate s measured from the vertex of the cone to the point in question.

In this investigation, we will not consider the conical frustum of Fig. 1(a), since it has already been shown [7] that the likelihood of buckling in the conical shell is relatively small, and that the tensile hoop stresses that develop in the lower parts of the conical shell can be adequately controlled through shell-thickness enhancement and the provision of tensile reinforcement.

Fig. 2 shows the loading and geometric parameters of the spherical dome, the paraboloid of revolution and the parabolic toroid. The profile of the spherical dome is a circular arc of radius a, while the cross-sectional profiles of the paraboloid of revolution and the parabolic toroid may be described by the equation $y = kx^2$ in Cartesian coordinates, with the tangent of the meridional angle ϕ representing the slope of the curve (dy/dx) at any given point.

The analytical results for membrane stresses in the three shells (as well as in the conical shell) may be seen in the earlier work [7]. Here, we will only cite the results for hydrostatic loading, which we will need later in considerations of the bending of the shell in the vicinity of the support. With γ denoting the weight per unit volume of the water, the parameters r_1 and r_2 for the three shells, and the membrane stress resultants due to hydrostatic pressure, are as follows [7]:

Spherical dome

$$r_1 = r_2 = a \tag{2}$$

$$N_\phi^m = -\frac{\gamma a^2}{6} \left[\left(\frac{1-\cos\phi}{1+\cos\phi} \right) (1 + 2\cos\phi) + \frac{3h_o}{a} \right] \tag{3a}$$

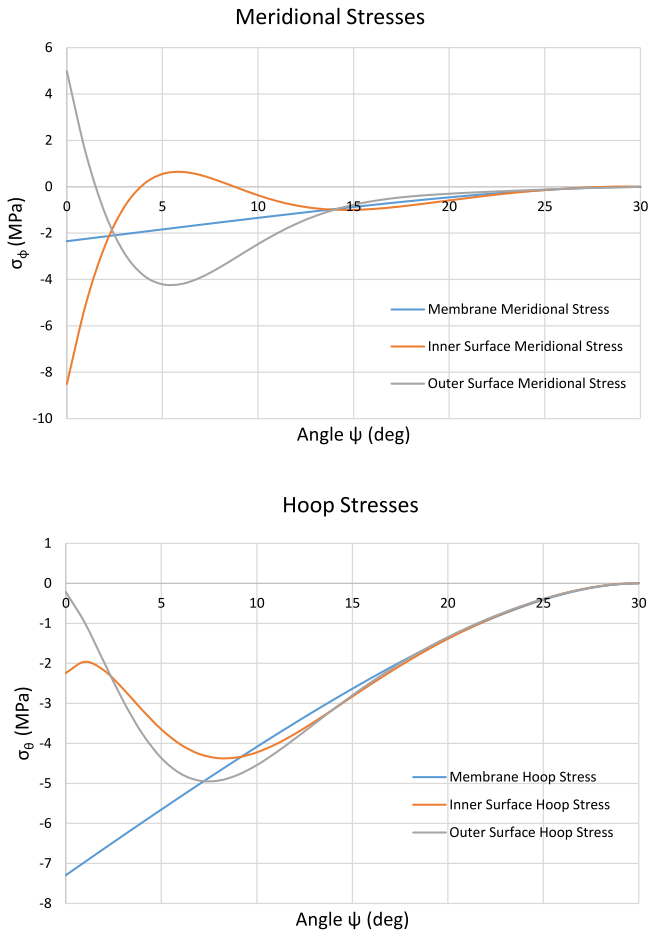

Fig. 7. Variation of net stresses (bending + membrane) with angle ψ measured from the shell edge, for the spherical dome with a fixed edge, and having geometric parameters a = 60 m, ϕ_s = 30°, t_o = 0.2 m and t_s = 0.5 m: (a) meridional stresses; (b) hoop stresses. Superscripts m, T(i) and T(o) denote membrane-solution stress, inner-surface total stress and outer-surface total stress, respectively.

$$N_\theta^m = -\frac{\gamma a^2}{6}\left[\left(\frac{1-\cos\phi}{1+\cos\phi}\right)(5+4\cos\phi)+\frac{3h_o}{a}\right] \tag{3b}$$

Paraboloid of revolution

$$r_1 = \frac{1}{2k\cos^3\phi}\ ; \quad r_2 = \frac{1}{2k\cos\phi} \tag{4a,b}$$

$$N_\phi^m = -\frac{\gamma}{32k^2}\left(\frac{\cos\phi}{\sin^2\phi}\right)\left[\frac{1}{\cos^4\phi}-2\left(\frac{1}{\cos^2\phi}\right)\left(\frac{1}{\cos^2\phi_w}\right)+\frac{1}{\cos^4\phi_w}\right] \tag{5a}$$

$$N_\theta^m = -\frac{\gamma}{32k^2}\left[4\left(\frac{\tan^2\phi-\tan^2\phi_w}{\cos\phi}\right)-\left(\frac{\cos\phi}{\tan^2\phi}\right) \times\left\{\frac{1}{\cos^4\phi}-2\left(\frac{1}{\cos^2\phi}\right)\left(\frac{1}{\cos^2\phi_w}\right)+\frac{1}{\cos^4\phi_w}\right\}\right] \tag{5b}$$

Parabolic toroid

$$r_1 = \frac{1}{2k\cos^3\phi}\ ; \quad r_2 = \frac{2kA\cos\phi-\sin\phi}{2k\cos\phi\sin\phi} \tag{6a,b}$$

$$N_\phi^m = -\frac{\gamma}{8k^2}\left(\frac{\cot\phi}{2kA\cos\phi-\sin\phi}\right)\left[2kA\right.$$

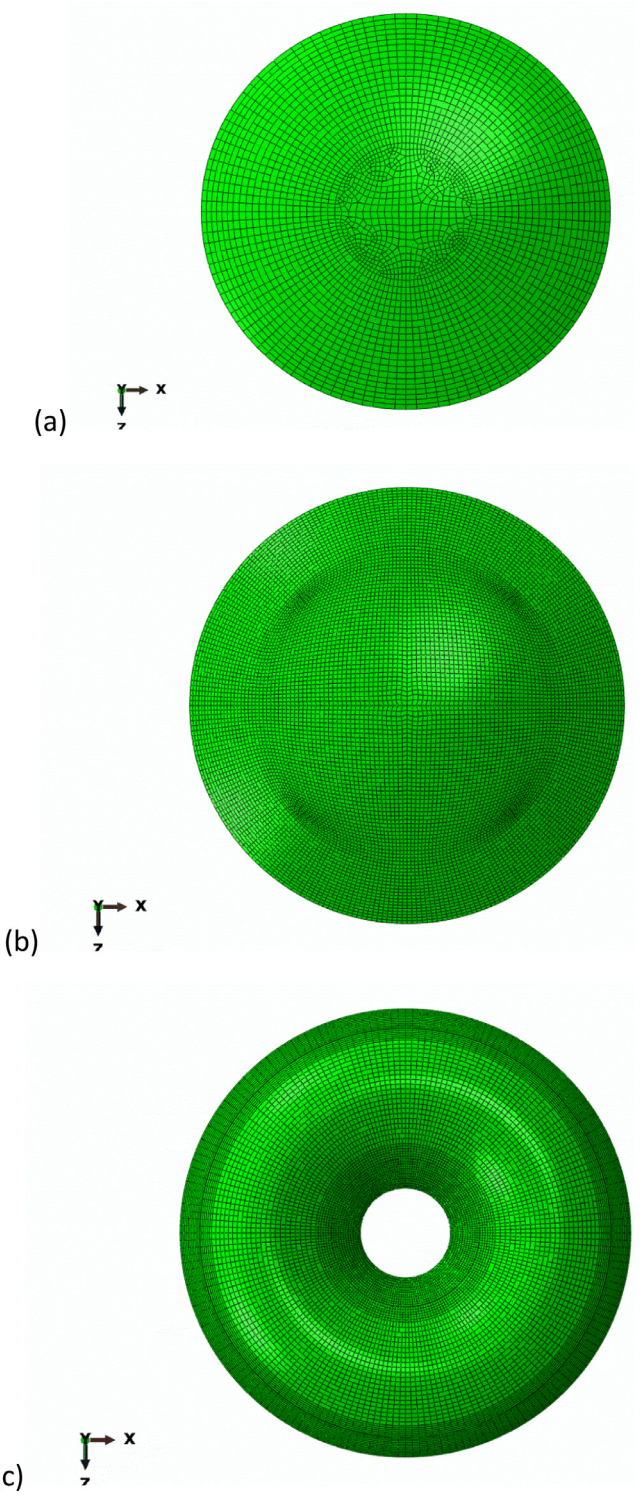

Fig. 8. Finite element meshes: (a) spherical dome (3122 elements); (b) paraboloid of revolution (10 384 elements); (c) parabolic toroid (11 280 elements).

$$\times\left\{\frac{\tan^3\phi}{3}-(\tan\phi)\left(\tan^2\phi_w\right)\right\} -\frac{1}{4}\left(\frac{1}{\cos^4\phi}+\frac{1}{\cos^4\phi_w}\right) +\frac{1}{2\left(\cos^2\phi\right)\left(\cos^2\phi_w\right)} +\frac{4kA}{3}\tan^3\phi_w\Big] \tag{7a}$$

Table 1
Values of parameters of the spherical dome.

Description	Value
Plan diameter of dome	$D = 60$ m
Rise of dome	$\eta = 8.04$ m
Rise-to-diameter ratio	$\eta/D = 0.134$
Radius of spherical shell	$a = 60$ m
Minimum shell thickness (at crest)	$t_o = 0.2$ m
Radius-to-thickness ratio (at crest)	$a/t_o = 300$
Water head at crest	$h_o = 0$
Support angle	$\phi_s = 30°$
Vertical loading intensity	$q = 10\,\text{kN/m}^2$

Table 2
Values of parameters of the paraboloid of revolution.

Description	Value
Plan diameter of dome	$D = 100$ m
Horizontal coordinate of support	$x_s = 50$ m
Vertical coordinate of support	$y_s = 20$ m
Angular coordinate of support	$\phi_s = 38.7°$
Horizontal coordinate of water level	$x_w = 35.36$ m
Vertical coordinate of water level	$y_w = 10$ m
Angular coordinate of water level	$\phi_w = 29.5°$
Minimum shell thickness (at crest)	$t_o = 0.1$ m
Vertical loading intensity	$q = 5\,\text{kN/m}^2$

$$N_\theta^m = \frac{\gamma}{8k^2}\left[\left(\frac{2kA\cos\phi - \sin\phi}{\cos\phi\sin\phi}\right) \times \left(\tan^2\phi - \tan^2\phi_w\right) - \left(\cot^2\phi\right)(\cos\phi) \times \left[2kA\left\{\frac{\tan^3\phi}{3} - (\tan\phi)\left(\tan^2\phi_w\right)\right\} - \frac{1}{4}\left(\frac{1}{\cos^4\phi} + \frac{1}{\cos^4\phi_w}\right) + \frac{1}{2\left(\cos^2\phi\right)\left(\cos^2\phi_w\right)} + \frac{4kA}{3}\tan^3\phi_w\right]\right] \tag{7b}$$

4. Parametric study

In the previous study [7], numerical examples were considered and membrane stresses evaluated, for the three shell geometries shown in Fig. 2. Increasing shell thickness was proposed as the simplest way of reducing the likelihood of buckling in zones of high compression. In the present study, we will pursue the same numerical examples. The thickness of the shell is increased *linearly* with respect to arc length measured along the meridian of the shell, from a minimum value of $t = t_o$ at the crest of the spherical dome (or the water level in the case of the parabolic dome and the toroidal dome), to a maximum value of $t = t_s$ at the level of the support. Thus, once numerical values have been assigned to the parameters t_o and t_s, the thickness of the shell throughout the dome is completely defined. In the case of the spherical dome, arc length from the crest of the dome (i.e. from $\phi = 0$) is, of course, directly proportional to the meridional angle ϕ, so the change in shell thickness (as we move from the crest) is directly proportional to the angle ϕ.

Numerical values of the parameters of the selected shells are listed in Tables 1 to 3, with subscript s referring to the location of the support, and subscript w referring to the location of the water level. The primary geometric parameters of the domes are illustrated in Fig. 2, to which the reader should refer. Secondary parameters (such as D and η) are as defined in the tables; they are not required in the calculations, and are only included to give a sense of the overall proportions of the domes.

In the tables, the parameter q refers to the vertical loading per unit area of the shell mid-surface, which may stem from the self-weight of the shell, or the weight of cladding on the shell (imposed dead load). For the purpose of the membrane analysis, this loading q may be resolved into a radial component (p_r) and a tangential component (p_ϕ), as shown in Fig. 2.

Table 3
Values of parameters of the parabolic toroid.

Description	Value
Mean toroidal radius	$A = 15$ m
Width of cross-section at base	$D = 20$ m
Horizontal coordinate of support	$x_s = 10$ m
Vertical coordinate of support	$y_s = 10$ m
Angular coordinate of support	$\phi_s = 63.4°$
Horizontal coordinate of water level	$x_w = 7.07$ m
Vertical coordinate of water level	$y_w = 5.0$ m
Angular coordinate of water level	$\phi_w = 54.7°$
Minimum shell thickness (at crest)	$t_o = 0.05$ m
Vertical loading intensity	$q = 5\,\text{kN/m}^2$

For the spherical dome, the shell thickness t is linearly varied with arc length along the meridian, from $t = t_o = 0.2$ m at the crest of the dome, to $t = t_s$ at the support, where t_s is assigned five values: $t_s = 0.3$ m; $t_s = 0.4$ m; $t_s = 0.5$ m; $t_s = 0.6$ m; $t_s = 0.7$ m. For the paraboloid of revolution, the shell thickness t is kept constant at $t_o = 0.1$ m in the range $0 \le \phi \le \phi_w$, then linearly varied with arc length along the meridian, from $t = t_o = 0.1$ m at the water level, to $t = t_s$ at the support, where t_s is assigned five values: $t_s = 0.50$ m; $t_s = 0.75$ m; $t_s = 1.00$ m; $t_s = 1.25$ m; $t_s = 1.50$ m. For the parabolic toroid, the shell thickness t is kept constant at $t_o = 0.05$ m in the range $0 \le \phi \le \phi_w$, then linearly varied with arc length along the meridian, from $t = t_o = 0.05$ m at the water level, to $t = t_s$ at the support, where t_s is assigned four values: $t_s = 0.10$ m; $t_s = 0.15$ m; $t_s = 0.20$ m; $t_s = 0.25$ m.

Membrane stresses σ_ϕ^m and σ_θ^m were evaluated at various points along the shell meridian, and plotted versus arc length s for various levels of local thickening. Some representative variations are shown in Figs. 3–5. For the full set of results, and a detailed discussion of these, reference must be made to the previous study [7]. At locations well below the water level, it is evident that the hydrostatic loading component accounts for most of the stress value. The benefits of varying shell thickness are also evident in all the plots. Gradual thickening of the shell with increasing hydrostatic pressure has the effect of countering the steep rates of increase of stresses σ_ϕ^m and σ_θ^m as the support is approached. The result of this gradual thickening is that the eventual stresses at the support are considerably lower than the stresses that would occur if a constant thickness t_o were maintained throughout the dome.

5. Bending stresses

The spherical dome, the parabolic dome and the toroidal dome are all shells of double curvature If the shells are sufficiently thin and not too shallow, the Reissner–Meissner pair of differential equations for the axisymmetric bending of general shells of revolution may be drastically simplified without too much loss in accuracy, by dropping all derivatives of order higher than two, and combining the ensuing equations into one fourth-order ordinary differential equation in the transverse-shear variable Q_ϕ:

$$\frac{d^4Q_\phi}{d\phi^4} + 4\lambda^4\,Q_\phi = 0 \tag{8}$$

where λ is the shell slenderness parameter defined as follows:

$$\lambda^4 = 3\left(1-\nu^2\right)\frac{r_1^4}{r_2^2t^2} \tag{9}$$

The accuracy of the above simplification for the specific case of the spherical shell has been shown to be very good (errors generally less than 5%) if $\phi_e \ge 30°$ and $a/t \ge 50$ [41]. For general shells of revolution, the same level of accuracy may be expected provided that $\phi_e \ge 30°$

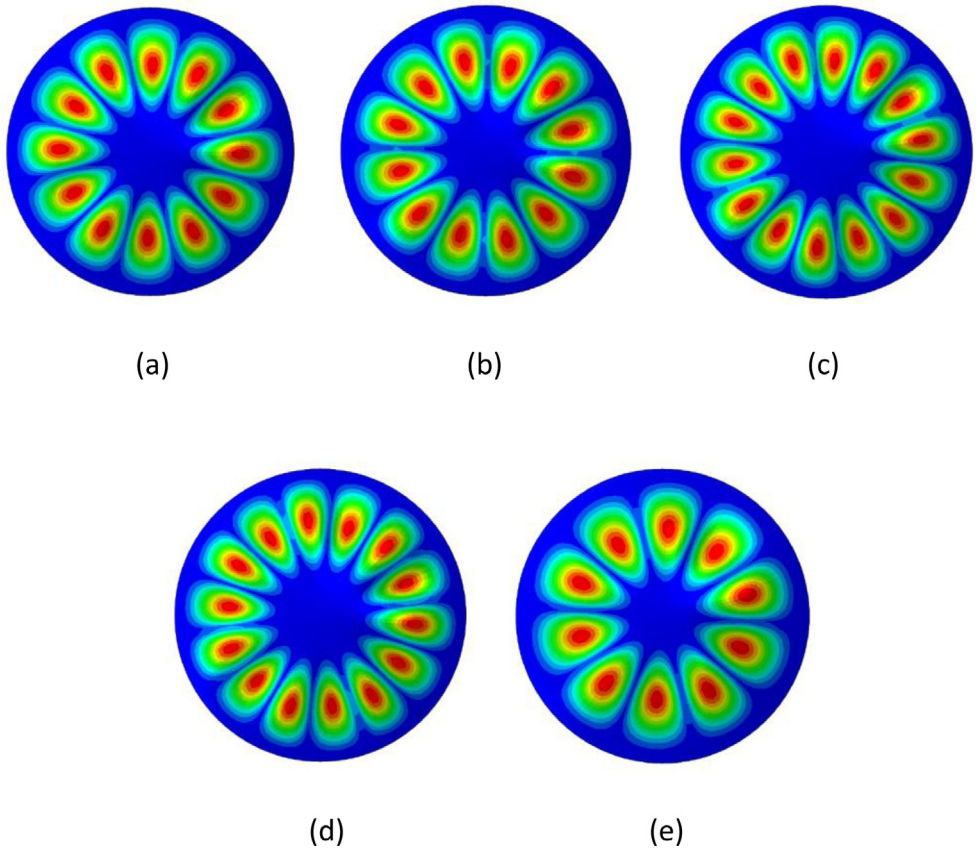

Fig. 9. First five modes of spherical dome with $t_s = 0.7$ m: (a) mode 1 ($\lambda = 62.04$); (b) mode 2 ($\lambda = 62.04$); (c) mode 3 ($\lambda = 64.06$); (d) mode 4 ($\lambda = 64.06$); (e) mode 5 ($\lambda = 64.32$).

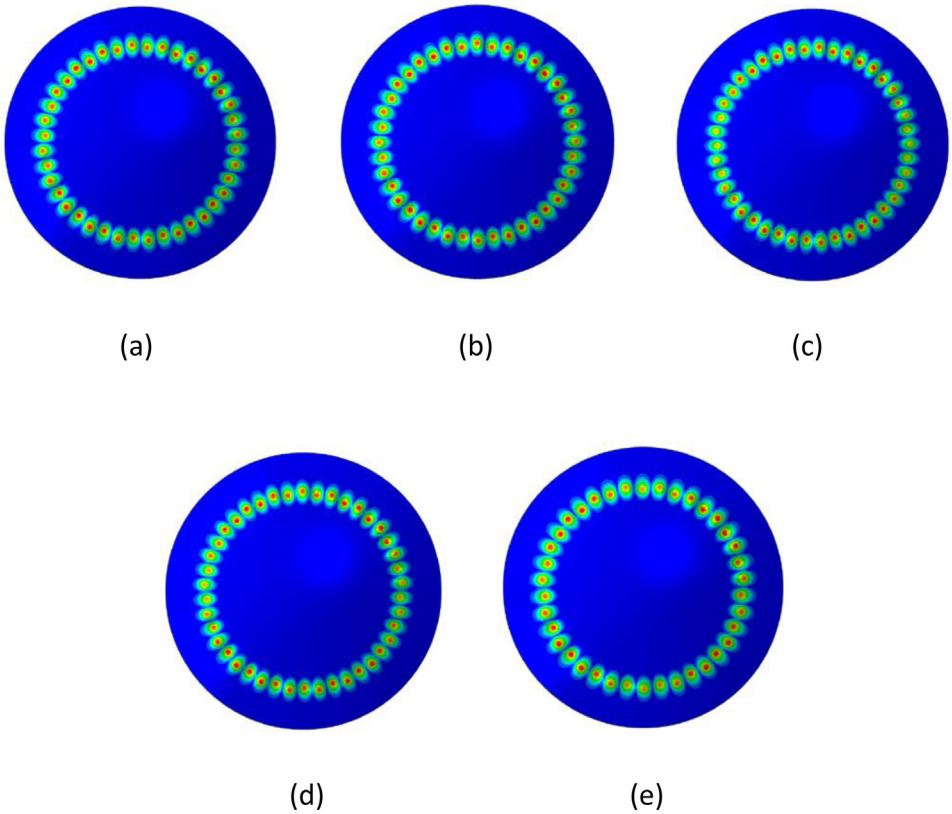

Fig. 10. First five modes of paraboloid of revolution with $t_s = 1.5$ m: (a) mode 1 ($\lambda = 30.08$); (b) mode 2 ($\lambda = 30.08$); (c) mode 3 ($\lambda = 30.11$); (d) mode 4 ($\lambda = 30.11$); (e) mode 5 ($\lambda = 30.14$).

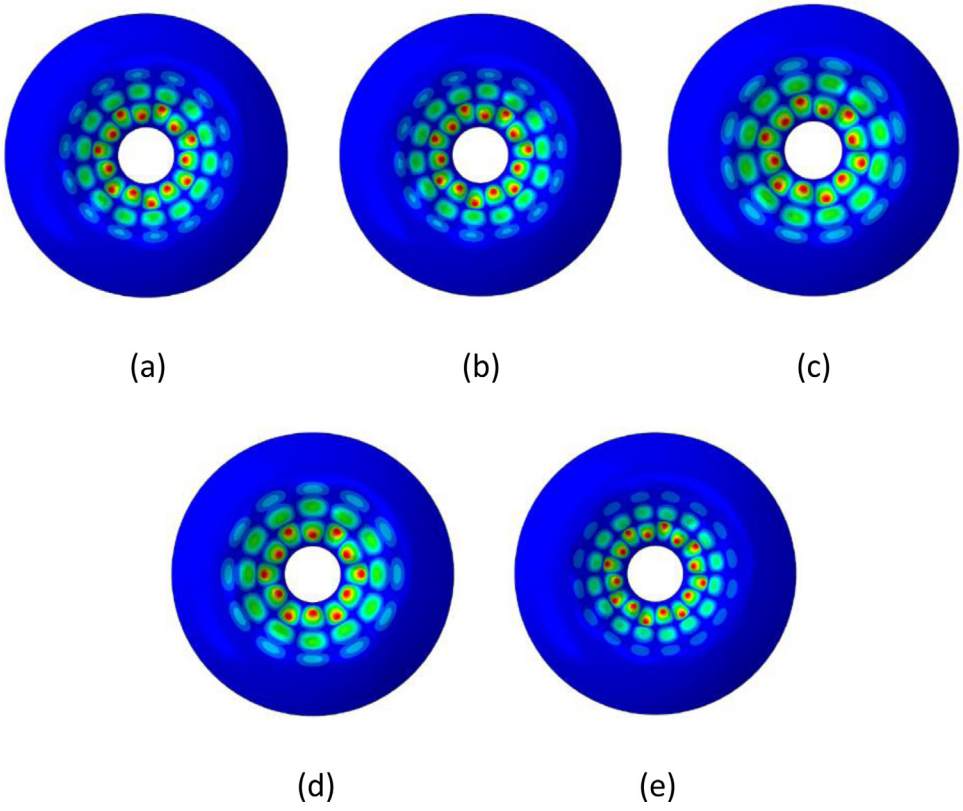

Fig. 11. First five modes of parabolic toroid with $t_s = 0.25$ m: (a) mode 1 ($\lambda = -72.45$); (b) mode 2 ($\lambda = -72.46$); (c) mode 3 ($\lambda = -74.47$); (d) mode 4 ($\lambda = -74.47$); (e) mode 5 ($\lambda = -76.40$).

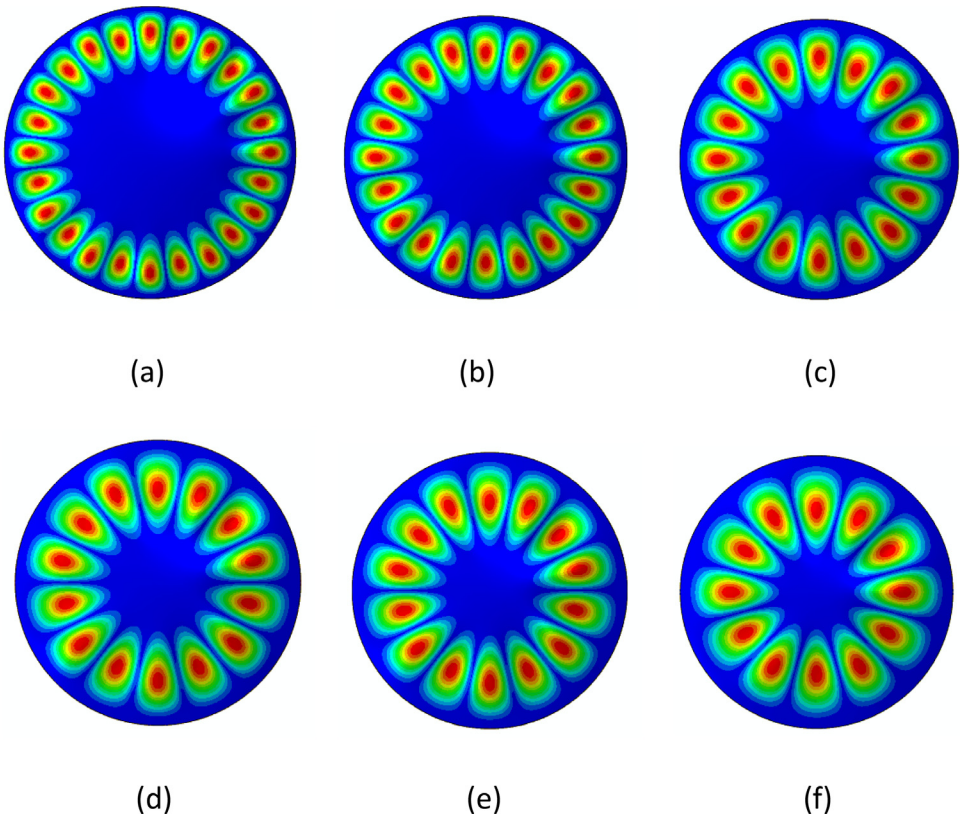

Fig. 12. Mode 1 of spherical dome for various values of t_s: (a) $t_s = 0.2$ m ($\lambda = 6.09$); (b) $t_s = 0.3$ m ($\lambda = 12.69$); (c) $t_s = 0.4$ m ($\lambda = 21.64$); (d) $t_s = 0.5$ m ($\lambda = 32.81$); (e) $t_s = 0.6$ m ($\lambda = 46.23$); (f) $t_s = 0.7$ m ($\lambda = 62.04$).

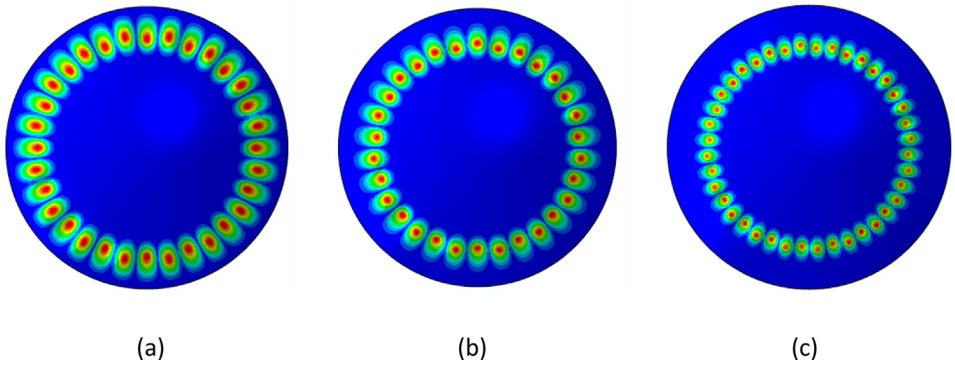

Fig. 13. Mode 1 of paraboloid of revolution for various values of t_s: (a) $t_s = 0.5$ m ($\lambda = 5.46$); (b) $t_s = 1.0$ m ($\lambda = 16.47$); (c) $t_s = 1.5$ m ($\lambda = 30.08$).

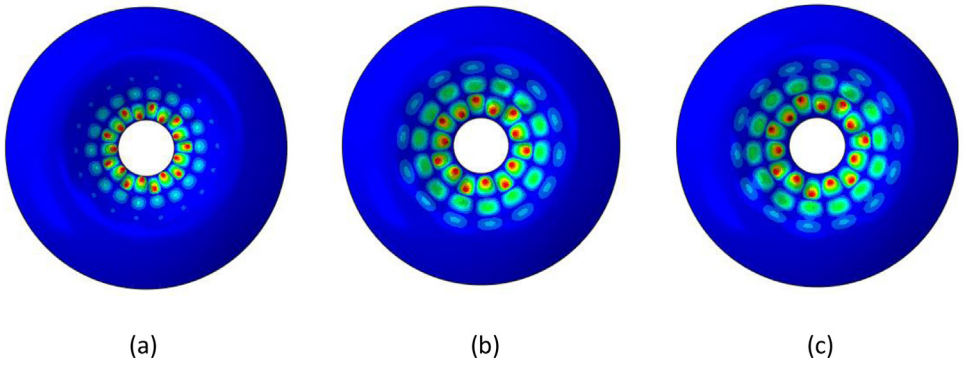

Fig. 14. Mode 1 of parabolic toroid for various values of t_s: (a) $t_s = 0.05$ m ($\lambda = -6.88$); (b) $t_s = 0.15$ m ($\lambda = -30.61$); (c) $t_s = 0.25$ m ($\lambda = -72.45$).

Table 4
Finite-element method (FEM) versus analytical (ANA) results for meridional stresses.

Angle ψ (deg)	Stress on outer surface (MPa)			Stress on inner surface (MPA)		
	ANA	FEM	% Diff	ANA	FEM	% Diff
0	4.99	5.12	2.5	−8.51	−8.85	3.8
2	−1.15	−1.25	8.0	−2.54	−2.65	4.2
4	−3.81	−3.92	2.8	0.10	0.20	50
6	−4.20	−4.34	3.2	0.64	0.75	14.7
8	−3.48	−3.60	3.3	0.24	0.35	31.4
10	−2.47	−2.56	3.5	−0.37	−0.44	15.9

at the edge of the shell, and $r_{\min}/t \geq 50$, where $r_{\min}$ is the smaller of r_1 and r_2. The spherical dome (with $\phi_s = 30°$ and $a/t_s = 85.7$ in the least favourable case of $t_s = 0.7$ m) fulfils both criteria. By reference to Table 2, and making use of Eqs. (4) to calculate the principal radii of curvature, we note that the paraboloid of revolution has $\phi_s = 38.7°$ and $r_{\min}/t_s = 53.39$ at the support (noting that $r_1 = 131.49$ m and $r_2 = 80.08$ m at the edge of the shell, and using the least favourable value of $t_s = 1.5$ m), so it also fulfils the criteria for the above approximation. However, caution needs to be used in applying the approximation to the parabolic toroid, because the dome may not be thin enough for certain ranges of t_s. From Table 3, $\phi_s = 63.4°$, which clearly fulfils the criterion for non-shallowness. Eqs. (6) yield $r_1 = 55.70$ m and $r_2 = 5.61$ m at the edge of the shell, so that $r_{\min}/t_s = 22.4$ at the support, based on the least favourable thickness value of $t_s = 0.25$ m. This clearly falls short of the criterion for thin-ness. To meet the criterion for thin-ness, $t_s \leq 0.112$ m. If toroidal radius A was larger, this would make r_2 bigger (see Eq. (6b)), which would bring the toroid closer to the range of sufficiently-thin shells.

In general, the principal radii of curvature r_1 and r_2 are functions of ϕ (except in the case of the spherical dome where $r_1 = r_2 = a$), and shell thickness t is also a function of ϕ in the edge regions (owing to gradual shell thickening). Thus the slenderness parameter λ (Eq. (9)) is a function of ϕ, implying that the second term of the differential equation (Eq. (8)) has a variable coefficient, and is therefore not so easy to solve. We may make a further simplication without too much loss in accuracy, by adopting a constant (average) value of λ in the edge zone. This is valid, since the zone experiencing edge effects is very narrow, and the parameters $\{r_1, r_2, t\}$ do not change much across the narrow band in which the edge effect prevails.

Now, the effective range ψ_r of the bending disturbance from the edge of the shell may arbitrarily be taken as the half-wavelength of its oscillations. Alternatively, the distance over which the function $e^{-\lambda\psi}$ (controlling the amplitude of these oscillations) decays from unity at the edge ($\psi = 0$) to 0.05 (i.e. 5% of initial value) may be adopted as the effective range. These two different criteria correspond to $\lambda\psi = \pi$ and $\lambda\psi = 3$ respectively, and therefore lead to essentially the same result, since $\pi \approx 3$. It is preferred to define the effective range of the bending disturbance as $\psi_r = \pi/\lambda$, or $180°/\lambda$.

To obtain the effective value of λ for use in the solution of Eq. (8), we start by calculating λ_s from Eq. (9), based on the value of $\{r_1, r_2, t\}$ at the supported edge of the shell. The support circle (where $\phi = \phi_s$) defines the lower boundary of the effective bending zone. We then evaluate the effective range of the bending disturbance based on this value of λ_s, i.e. $\psi_r = \pi/\lambda_s$. Next, we calculate $\{r_1, r_2, t\}$ at the upper boundary of the effective bending zone, defined by the meridional angle $\phi_r = \phi_s - \psi_r$, and evaluate λ_r at that location, again using Eq. (9). The effective value of λ in the edge zone is simply the average of λ_s and λ_r.

For the partially-submerged domes, edge-disturbance interaction [42] is not a concern here, since the water level is associated with insignificant edge effects (in comparison with the support level), and, in any case, the two "edges" (i.e. the water level and the support level) are relatively far apart.

If we assume there is no surface loading on the shell, and only axisymmetric bending moments M_e (per unit length) and horizontal

(a)

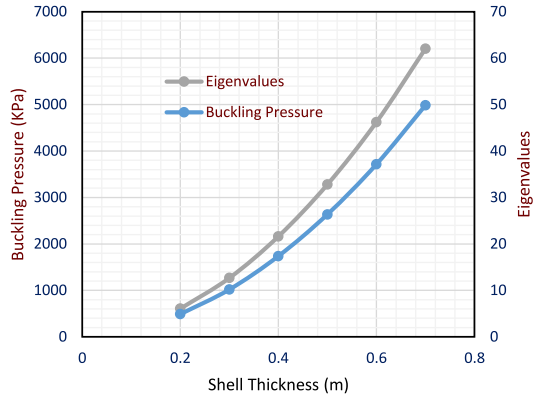

(b)

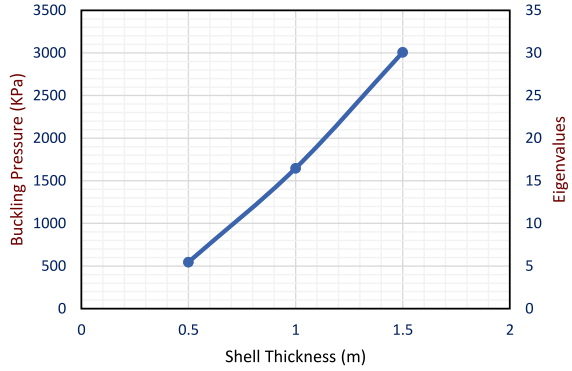

(c)

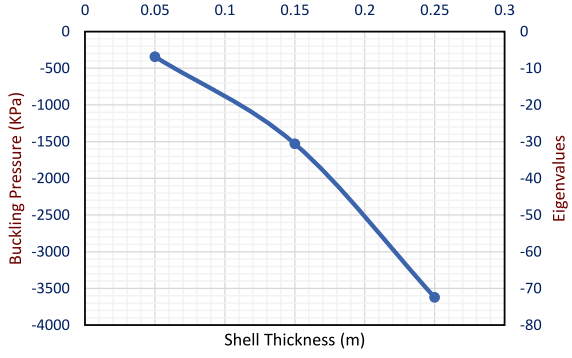

Fig. 15. Variation of linear shell-buckling capacity with chosen shell thickness t_s at the base: (a) spherical dome; (b) paraboloid of revolution; (c) parabolic toroid.

shear forces H_e (per unit length) act at the edge of the shell, the above simplified theory leads to the following results for edge deformations and interior shell actions due to the actions M_e and H_e [12]:

$$\begin{bmatrix} V_e^b \\ \delta_e^b \end{bmatrix} = \begin{bmatrix} -\dfrac{4\lambda^3}{Etr_1}\left(\dfrac{r_2^2}{r_1^2}\right) & \dfrac{2\lambda^2}{Et}\left(\dfrac{r_2^2}{r_1^2}\right)\sin\phi_e \\ \dfrac{2\lambda^2}{Et}\left(\dfrac{r_2^2}{r_1^2}\right)\sin\phi_e & -\dfrac{2\lambda}{Et}\left(\dfrac{r_2^2}{r_1}\right)\sin^2\phi_e \end{bmatrix} \begin{bmatrix} M_e \\ H_e \end{bmatrix} = \begin{bmatrix} I_{11} & I_{12} \\ I_{21} & I_{22} \end{bmatrix} \begin{bmatrix} M_e \\ H_e \end{bmatrix} \tag{10}$$

$$N_\phi^b = -\left\{\cot\left(\phi_e - \psi\right)\right\} e^{-\lambda\psi}\left[\frac{2\lambda}{r_1} M_e \sin\lambda\psi - H_e\left(\sin\phi_e\right)\left(\sin\lambda\psi - \cos\lambda\psi\right)\right] \tag{11a}$$

$$N_\theta^b = -2\left(\frac{r_2}{r_1}\right)\lambda\, e^{-\lambda\psi}\left[\frac{\lambda}{r_1} M_e\left(\sin\lambda\psi - \cos\lambda\psi\right) + H_e\left(\sin\phi_e\right)\cos\lambda\psi\right] \tag{11b}$$

$$M_\phi = e^{-\lambda\psi}\left[M_e\left(\sin\lambda\psi + \cos\lambda\psi\right) - \frac{r_1}{\lambda} H_e\left(\sin\phi_e\right)\sin\lambda\psi\right] \tag{11c}$$

$$M_\theta = \nu\, M_\phi \tag{11d}$$

In the flexibility matrix of the deformation relationships, the relationship $I_{1,2} = I_{2,1}$ is well-known. In general, while subscript e denotes the edge of the shell, we will use superscripts m and b to distinguish contributions of the membrane solution and the bending edge effects. Thus, the edge deformations associated with the membrane stress resultants will be denoted by $\{\delta_e^m, V_e^m\}$, while those associated with the bending edge effects will be denoted by $\{\delta_e^b, V_e^b\}$. The combined edge deformations (membrane + bending) will be denoted by $\{\delta_e^T, V_e^T\}$.

Shell-edge actions M_e and H_e are initially assumed to be unknowns. They may be evaluated through a flexibility-type approach by imposing conditions of compatibility. For this purpose, deformations at the shell edges, δ_e and V_e are required. If the edge of the shell coincides with the support location, we may use the designation δ_s and V_s for the edge deformations, and M_s and H_s for the edge actions. The positive conventions for edge deformations and edge actions are shown in Fig. 6, where the shell edge is attached to a ring beam at the support location. The equal and opposite reactions (M_s and H_s) on the ring beam are also shown. The force H_r^m is simply the horizontal component of the equal and opposite pull on the ring beam due to the membrane meridional stress resultant at the edge of the shell (assumed to be a tensile).

If a ring beam is provided at the base of the shell, compatibility of deformations requires that the ring beam and the shell rotate and translate by the same amount at their point of attachment. Let us consider the limiting boundary conditions of a *fixed* edge and a *hinged* edge at the base of the shell, where the hinge is a moment release ($M = 0$) that does not permit any translation. For a fixed edge (which is equivalent to attaching the shell to a ring beam of infinite rigidity), we apply upon the shell deformations the boundary conditions of zero lateral displacement and zero meridional rotation, to obtain the following solutions for the shell redundants:

$$M_e = \frac{I_{22} V_e^m - I_{12}\delta_e^m}{I_{12}^2 - I_{11} I_{22}} \tag{12a}$$

$$H_e = \frac{I_{11}\delta_e^m - I_{12} V_e^m}{I_{12}^2 - I_{11} I_{22}} \tag{12b}$$

In the above solutions, the flexibility coefficients $I_{i,j}$ ($i = 1, 2$; $j = 1, 2$) are as previously defined. The membrane deformations $\{\delta_e^m, V_e^m\}$ at the edge of the shell can easily be calculated, for any given loading on the shell. We first need to obtain expressions for membrane deformations $\{\delta^m, V^m\}$ at generalised locations defined by the coordinate ϕ, by substituting the relevant solutions for N_ϕ^m and N_θ^m into the following general relationships [12]:

$$\delta^m = \frac{1}{Et}\left(r_2 \sin\phi\right)\left(N_\theta^m - \nu N_\phi^m\right) \tag{13a}$$

$$V^m = \frac{1}{r_1}\left[\frac{\cot\phi}{Et}\left\{\left(r_1 + \nu r_2\right) N_\phi^m - \left(r_2 + \nu r_1\right) N_\theta^m\right\} - \frac{d}{d\phi}\left\{\frac{r_2}{Et}\left(N_\theta^m - \nu N_\phi^m\right)\right\}\right] \tag{13b}$$

For a pinned edge, the bending moment at the edge of the shell is zero, so M_e is automatically zero. We only need to apply the boundary condition of zero lateral displacement to obtain the solution for H_e, which is as follows:

$$H_e = -\frac{\delta_e^m}{I_{22}} \tag{14}$$

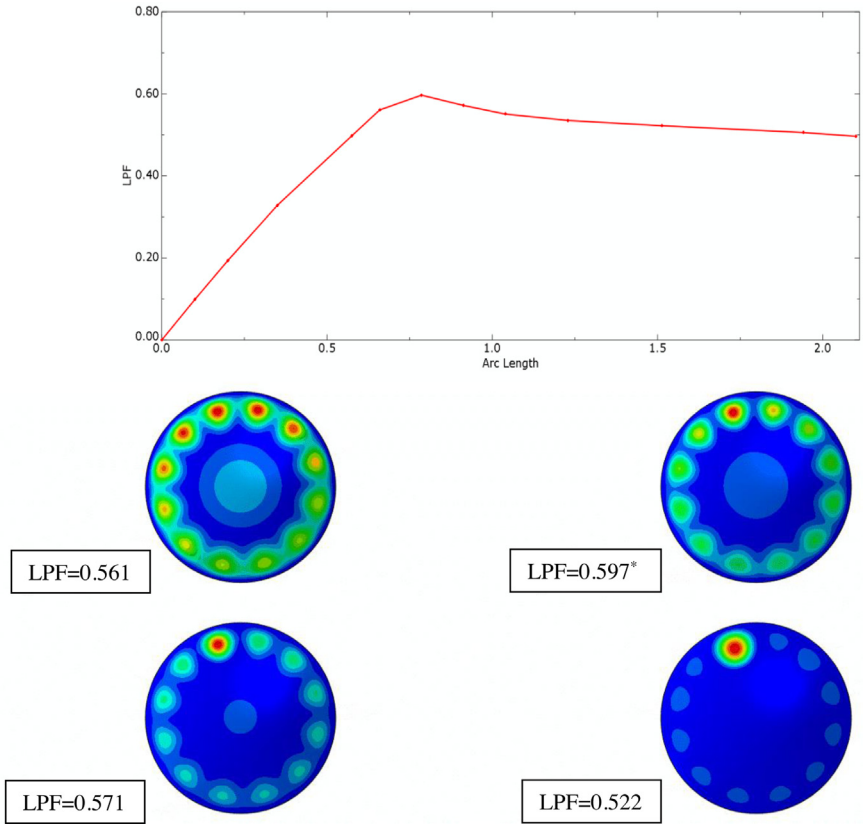

Fig. 16. Load factor (LPF) vs. arc-length and progressive development of deformation for the spherical dome: Case 1: $t_s = 0.2$ m. The asterisk (*) denotes peak load factor.

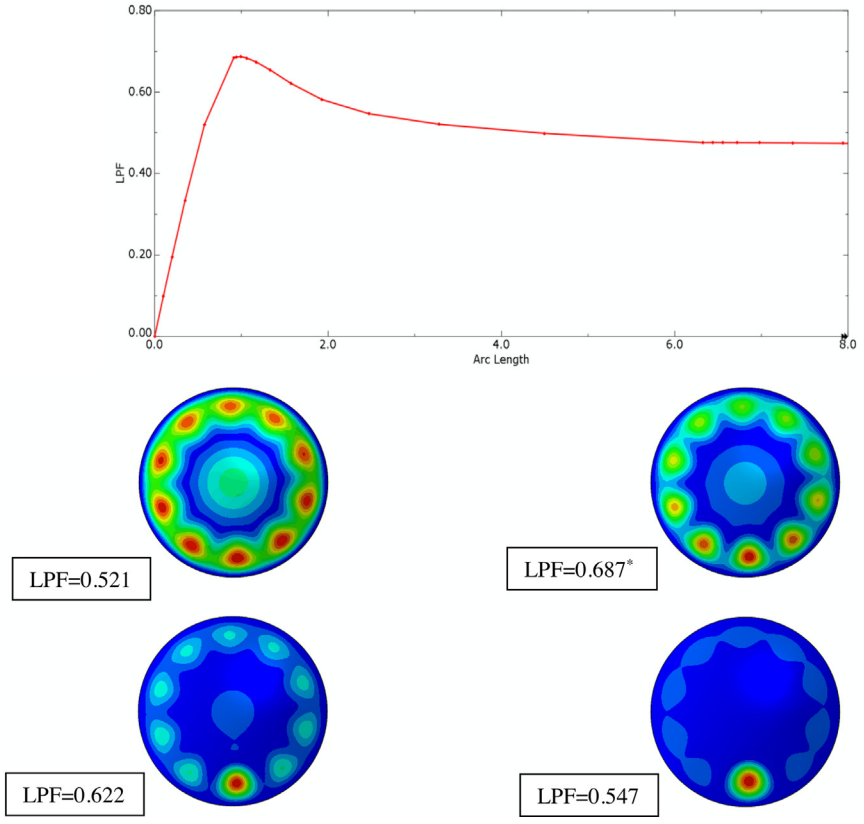

Fig. 17. Load factor (LPF) vs. arc-length and progressive development of deformation for the spherical dome: Case 2: $t_s = 0.3$ m. The asterisk (*) denotes peak load factor.

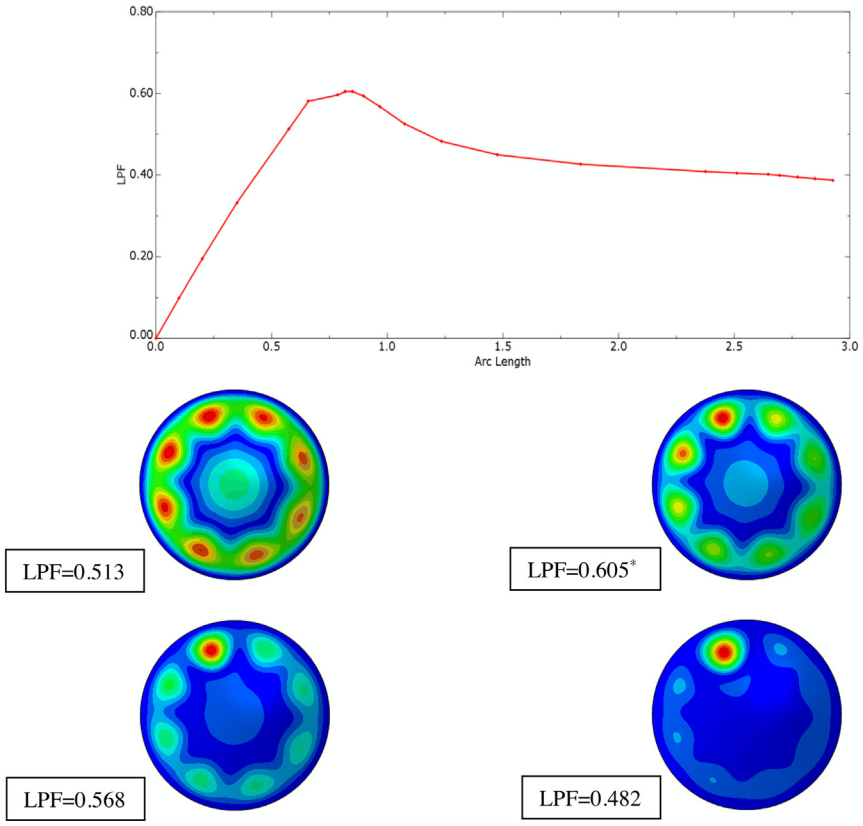

Fig. 18. Load factor (LPF) vs. arc-length and progressive development of deformation for the spherical dome: Case 3: $t_s = 0.4$ m. The asterisk (*) denotes peak load factor.

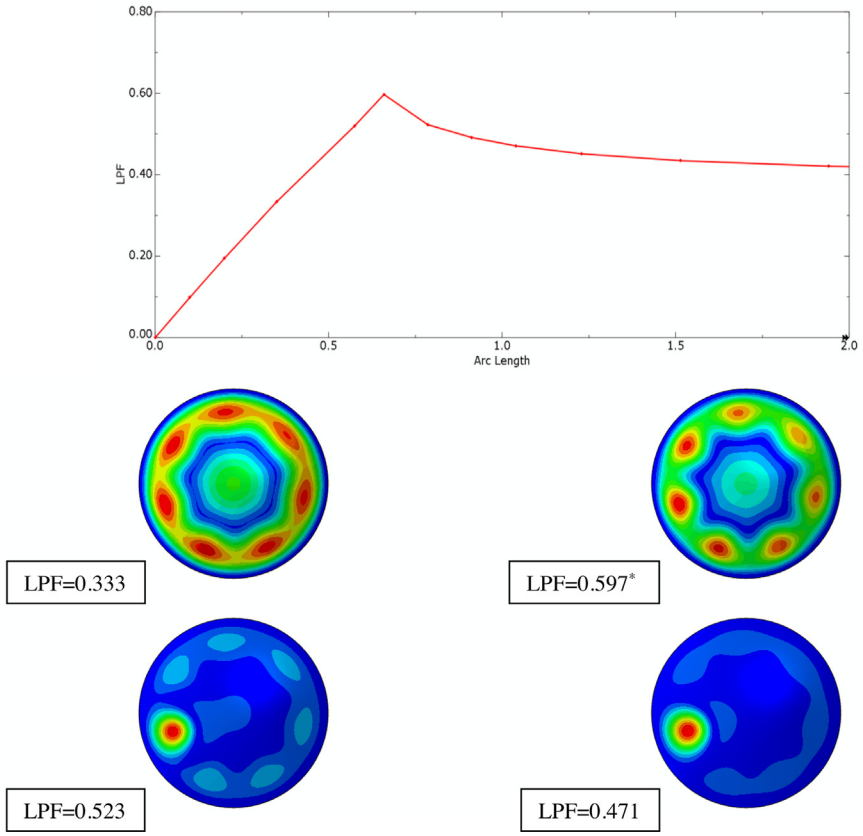

Fig. 19. Load factor (LPF) vs. arc-length and progressive development of deformation for the spherical dome: Case 4: $t_s = 0.5$ m. The asterisk (*) denotes peak load factor.

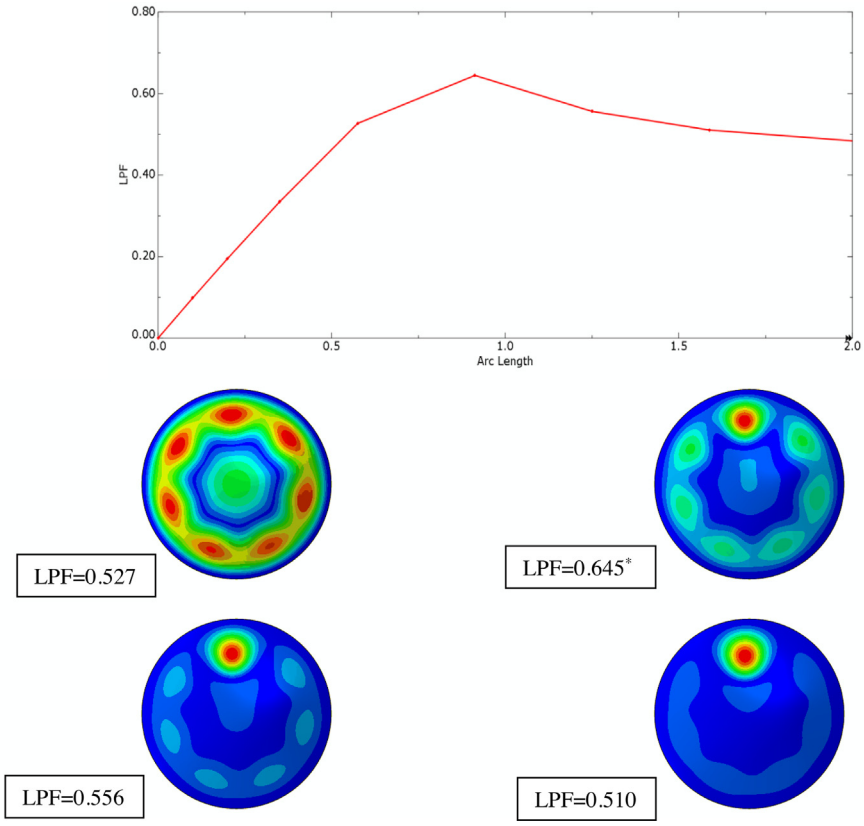

Fig. 20. Load factor (LPF) vs. arc-length and progressive development of deformation for the spherical dome: Case 5: $t_s = 0.6$ m. The asterisk (*) denotes peak load factor.

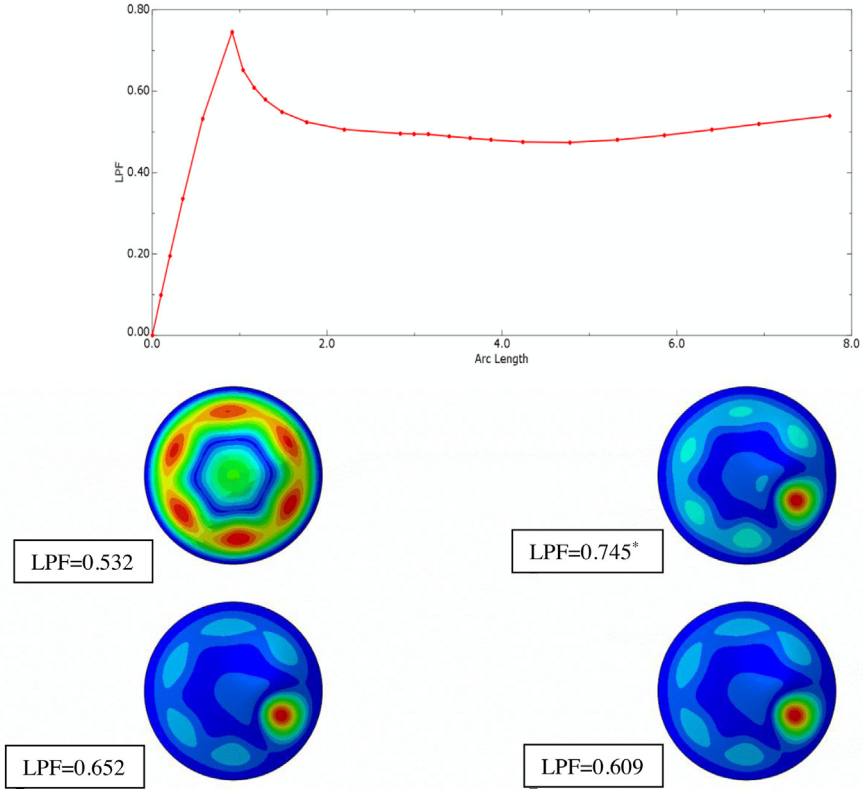

Fig. 21. Load factor (LPF) vs. arc-length and progressive development of deformation for the spherical dome: Case 6: $t_s = 0.7$ m. The asterisk (*) denotes peak load factor.

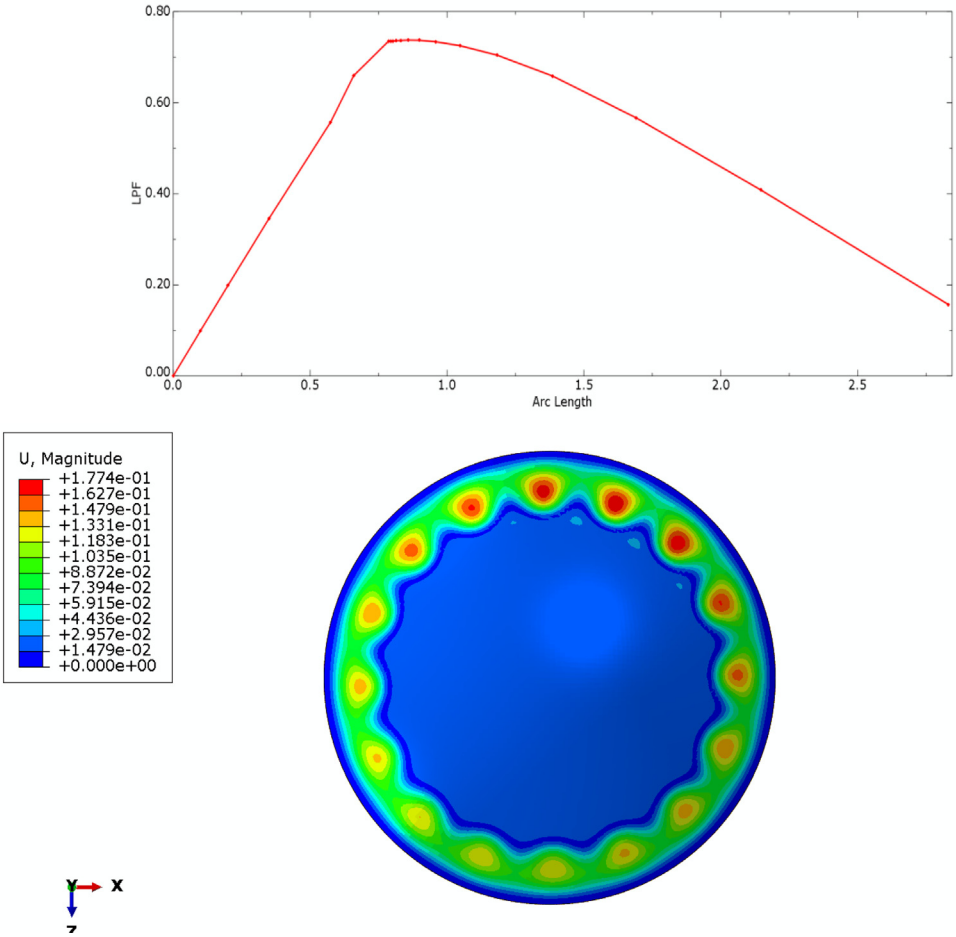

Fig. 22. Load factor (LPF) vs. arc-length for the paraboloid of revolution: Case 1: $t_s = 0.5$ m. The deformation image is taken at arc-length 0.958 and LPF 0.734.

To illustrate the derivation of edge deformations, let us consider the case of the spherical dome. The principal radii of curvature are independent of the angular coordinate ϕ (i.e. $r_1 = r_2 = a$), but the shell thickness t varies with meridional angle ϕ, which will affect the meridional rotation V^m. Let us express the linear variation of shell thickness with arc length as follows

$$t = t_o + \alpha\phi = t_o + \left(\frac{t_s - t_o}{\phi_s}\right)\phi \tag{15}$$

where t_o is the shell thickness at the crown ($\phi = 0$), t_s is the shell thickness at the support, ϕ_s is the value of ϕ at the support, and α is a constant of proportionality as implicitly defined above.

We derive expressions for hydrostatic-pressure membrane deformations by substituting into Eqs. (13) the solutions for the membrane stress resultants N_ϕ^m and N_θ^m as given by Eqs. (3), with h_o (the water head at the crest of the dome) taken as zero. Obtaining the result for δ^m only involves one simple substitution, but obtaining the result for V^m requires evaluation of derivatives of t, N_ϕ^m and N_θ^m with respect to ϕ, followed by some rather tedious but otherwise straightforward simplifications. Key derivational steps and final results are as follows:

$$\begin{aligned}\delta^m &= \frac{a}{Et}(\sin\phi)\left(N_\theta^m - \nu N_\phi^m\right)\\ &= -\frac{\gamma a^3}{6Et}(\sin\phi)\left(\frac{1-\cos\phi}{1+\cos\phi}\right)\{(5+4\cos\phi) - \nu(1+2\cos\phi)\}\end{aligned} \tag{16a}$$

$$\begin{aligned}V^m &= \frac{1+\nu}{Et}(\cot\phi)\left(N_\phi^m - N_\theta^m\right) - \frac{1}{Et}\frac{d}{d\phi}\left(N_\theta^m - \nu N_\phi^m\right) + \frac{\alpha}{Et^2}\left(N_\theta^m - \nu N_\phi^m\right)\\ &= \frac{\gamma a^2}{Et}(\sin\phi) + \frac{\alpha}{Et^2}\left(N_\theta^m - \nu N_\phi^m\right)\\ &= \frac{\gamma a^2}{Et}\left[(\sin\phi) - \left(\frac{t_s - t_o}{6t\phi_s}\right)\left(\frac{1-\cos\phi}{1+\cos\phi}\right)\{(5+4\cos\phi) - \nu(1+2\cos\phi)\}\right]\end{aligned} \tag{16b}$$

The required membrane deformations at the shell edge (which is the support location) follow by evaluating the general results for δ^m and V^m at the location $\phi = \phi_s$:

$$\delta_e^m = \delta_s^m = -\frac{\gamma a^3}{6Et_s}(\sin\phi_s)\left(\frac{1-\cos\phi_s}{1+\cos\phi_s}\right)\left\{\left(5+4\cos\phi_s\right) - \nu\left(1+2\cos\phi_s\right)\right\} \tag{17a}$$

$$\begin{aligned}V_e^m = V_s^m = \frac{\gamma a^2}{Et_s}\Bigg[&\left(\sin\phi_s\right) - \left(\frac{t_s - t_o}{6t_s\phi_s}\right)\left(\frac{1-\cos\phi_s}{1+\cos\phi_s}\right)\\ &\times\left\{\left(5+4\cos\phi_s\right) - \nu\left(1+2\cos\phi_s\right)\right\}\Bigg]\end{aligned} \tag{17b}$$

Once the bending-related edge actions M_e and H_e have been evaluated, the associated interior shell actions follow from Eqs. (11). The total stresses on the inner and outer surfaces of the shell are finally obtained by superimposing the membrane-solution stresses with those associated with the edge effect, taking care to use the value of shell thickness that applies at the location in question:

$$\sigma_\phi^T = \frac{N_\phi^m}{t} + \frac{N_\phi^b}{t} \pm \frac{6M_\phi}{t^2} \tag{18a}$$

$$\sigma_\theta^T = \frac{N_\theta^m}{t} + \frac{N_\theta^b}{t} \pm \frac{6M_\theta}{t^2} \tag{18b}$$

Let us pursue the spherical dome for a specific numerical example. Focusing attention on the case $t_s = 0.5$ m, with all other parameters of the spherical dome remaining the same as before (i.e. $a = 60$ m;

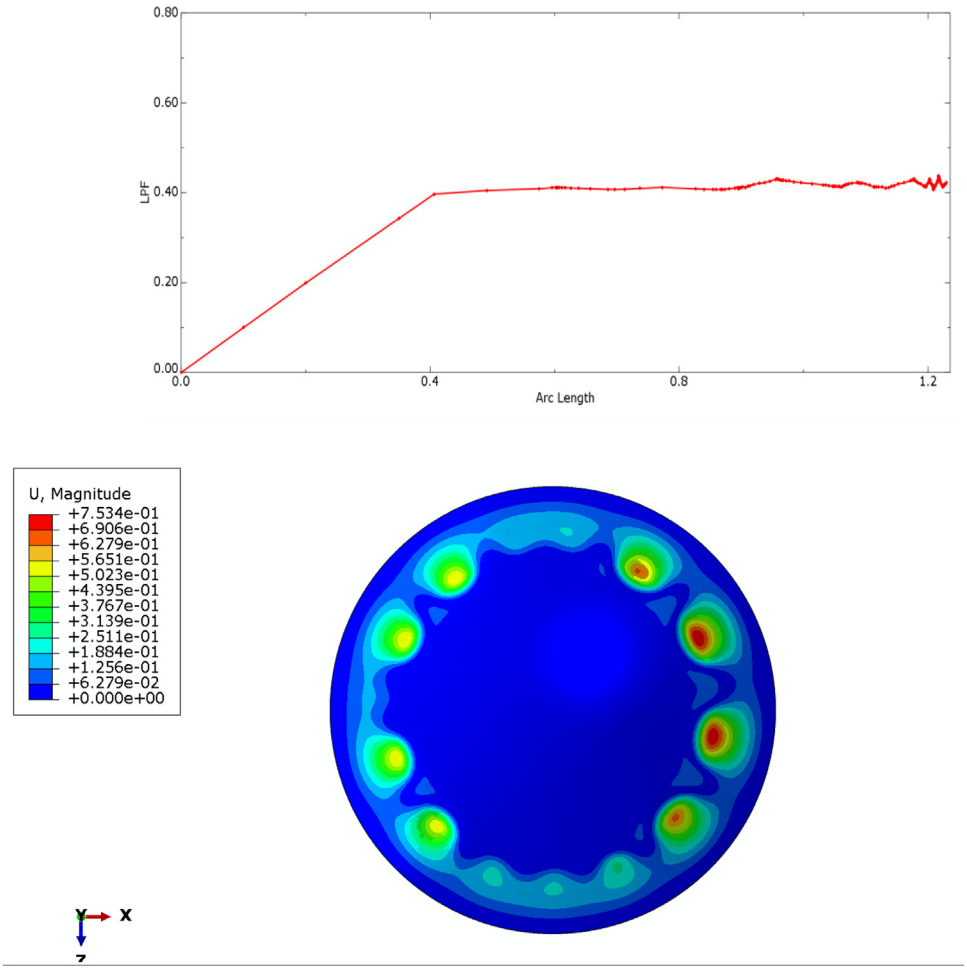

Fig. 23. Load factor (LPF) vs. arc-length for the paraboloid of revolution: Case 2: $t_s = 1.0$ m. The deformation image is taken at arc-length 1.069 and LPF 0.418.

$\phi_s = 30°$; $t_o = 0.2$ m), and the material properties of concrete taken as $E = 28 \times 10^9$ N/m^2 (Young's modulus) and $\nu = 0.15$ (Poisson's ratio), we may calculate the parameters $\{\lambda_s, \psi_r, t_r, \lambda_r\}$ as per the procedure described earlier, to give

$\lambda_s = 14.335$; $\psi_r = \pi/\lambda_s = 0.2192 = 12.56°$; $\phi_r = \phi_s - \psi_r = 17.44°$;
$t_r = 0.374$ m; $\lambda_r = 16.575$

The effective values of shell-slenderness parameter and shell thickness over the effective range of the bending disturbance are the averages of the values at the support ($\psi = 0$) and at $\psi = \psi_r$:

$\lambda_{av} = 0.5\,(\lambda_s + \lambda_r) = 15.455$; $t_{av} = 0.5\,(t_s + t_r) = 0.437$ m

Using these average values of λ and t, the flexibility coefficients of the spherical shell are evaluated from Eq. (10). The results are as follows:

$I_{11} = -2.0113 \times 10^{-8}$ N^{-1}
$I_{12} = I_{21} = 1.9521 \times 10^{-8}$ m N^{-1}
$I_{22} = -3.7892 \times 10^{-8}$ m^2 N^{-1}

The membrane deformations at the support are evaluated from Eqs. (17). The results are:

$\delta_e^m = \delta_s^m = -7.4349 \times 10^{-3}$ m
$V_e^m = V_s^m = 1.00172 \times 10^{-3}$

Let us assume the spherical dome has a fixed edge at the base. Evaluating the shell-edge actions from Eqs. (12), we obtain the results:

$M_e = -281\,272$ N m/m $= -281.272$ kN m/m

$H_e = -341\,117$ N/m $= -341.117$ kN/m

Substituting these values for M_e and H_e into expressions (11), we obtain the bending-related interior actions $\left\{N_\phi^b;\ N_\theta^b;\ M_\phi;\ M_\theta\right\}$; when the associated stresses are combined with membrane stresses in accordance with Eq. (18), we obtain the total stresses in the shell. Fig. 7 shows meridional and hoop stresses plotted versus the angle ψ from the support. In each chart, variations of (i) membrane stress, (ii) total stress on the inner surface, and (iii) total stress on the outer surface, are shown. It should be noted that the bending-related total meridional stress is dominated by the flexural component due to the bending moment M_ϕ, hence the symmetry of the curves of the inner and outer surfaces relative to the membrane plot; the component of meridional stress due to the bending moment is effectively the total-stress curve read with the membrane-stress curve taken as the datum, so we do not need to show the stress variation due to bending moment (M_ϕ) separately.

In order to validate the analytical formulation presented in this section, the same numerical example of the spherical dome ($a = 60$ m; $\phi_s = 30°$; $t_o = 0.2$ m; $t_s = 0.5$ m) was also analysed using the general-purpose finite element programme ABAQUS [43]. As the geometry and loading are axisymmetric, and the deformation response of the shell is axisymmetric, quadratic axisymmetric thin shell elements SAX2 (with three nodes) were employed. The circular meridian of the shell ($0 \le \phi \le 30°$) was divided into 100 elements each subtending an angle of 0.3° at the centre of curvature of the shell, which gave an element length of 0.314 m. As the dome was assumed to have a fixed edge, all nodal degrees of freedom were assigned values of zero at the shell edge. Finite element (FEM) meridional stresses are shown versus their analytical

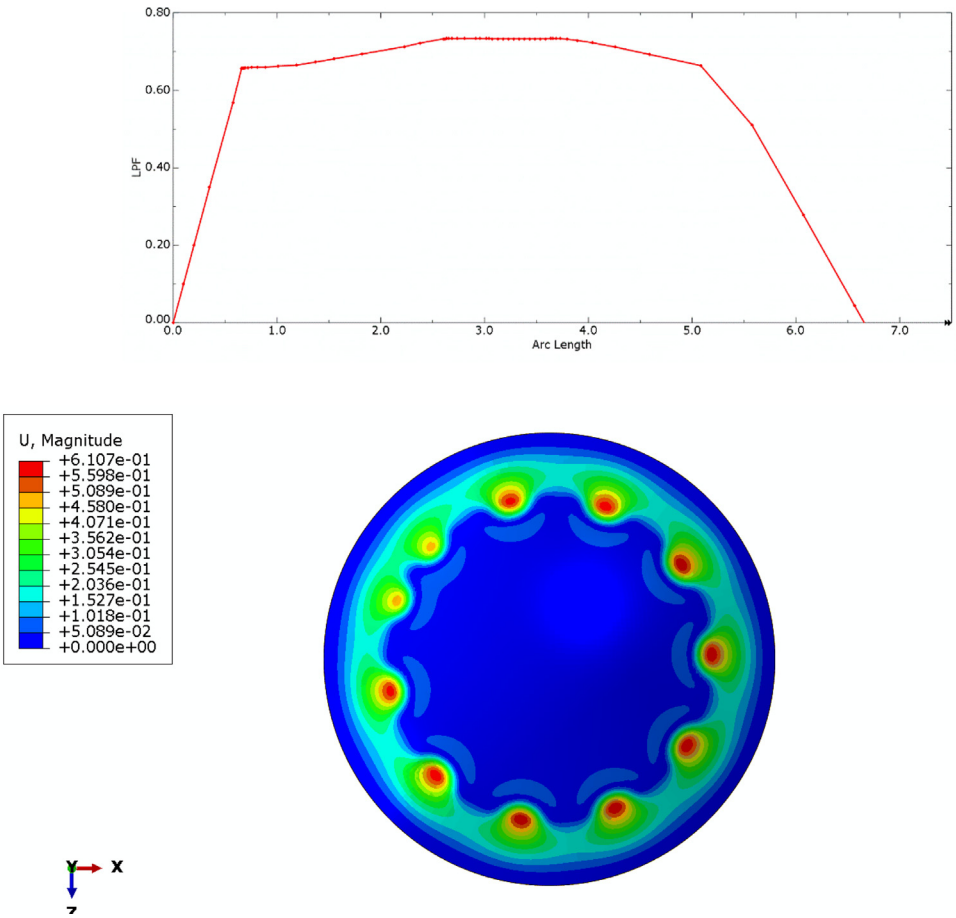

Fig. 24. Load factor (LPF) vs. arc-length for the paraboloid of revolution: Case 3: $t_s = 1.5$ m. The deformation image is taken at arc-length 4.26 and LPF 0.711.

(ANA) counterparts in Table 4. The discrepancy between FEM and analytical results is generally less than 5% (ignoring the percentages for stress levels that are insignificant (less than 1.0 MPa)), which confirms the validity of the analytical formulation, which is known to be of an approximate nature in any case.

It is clear that the edge effect significantly alters the membrane state of stress in the zone of the dome adjacent to the support. In the meridional direction, bending induces relatively large compressive and tensile stresses at the support (−8.51 MPa on the inner surface, and +4.99 MPa on the outer surface), compared with a membrane meridional-stress value of −2.35 MPa. On the other hand, the edge effect is beneficial on the hoop stresses: the membrane value of −7.29 MPa is lowered to −2.23 MPa on the inner surface and −0.21 MPa on the outer surface.

Although the increased thickness of the shell in the lower region of the dome has the effect of extending the effective range of the bending effects (since $\psi_r = \pi/\lambda$, and λ is reduced by shell thickening), it does have the beneficial effect of lowering the magnitude of the flexural stresses (since these are proportional to t^{-2}). Similar trends are observed in the case of the paraboloid of revolution and the parabolic toroid, though the bending disturbance decays somewhat more slowly in the case of the parabolic toroid, on account of its negative Gaussian curvature.

A common practice in concrete design is to assume the concrete does not have tensile strength. That means the oscillating bending stresses in the vicinity of the support should be catered-for by the provision of tensile reinforcement on *both* faces of the concrete section. The shell thickening that has been proposed also has the additional benefit of allowing the physical space for the placement of two layers of tensile reinforcement. It is recommended that these two layers be extended up to the effective range of the bending disturbance, as estimated earlier.

6. Eigenvalue buckling analysis

A linear eigenvalue buckling analysis of the three examples was performed using ABAQUS [43]. For the material (concrete), Young's modulus was taken as 28 GPa, and Poisson's ratio as 0.15. The shells were all assumed to be fixed at the base. The assumption of a fixed shell edge is valid if the ring beam at the base of the shell is sufficiently robust, or if the shell edge is built into a rigid concrete floor slab (which also helps to achieve watertightness at the junction of the shell and the reservoir floor). The fully integrated general-purpose quadrilateral shell element S4 was adopted on account of its accuracy. The spherical dome, the paraboloid of revolution and the parabolic toroid were discretised into 3122, 10 384 and 11 280 elements respectively. The generated meshes are shown in Fig. 8.

The reference pressure for the eigenvalue analysis was taken as $\gamma h_{\max}$ (taking γ as 10 kN/m^3), with $h_{\max}$ being the maximum depth of water. For the spherical dome, the paraboloid of revolution and the parabolic toroid, $h_{\max}$ is 8.038 m, 10.0 m and 5.0 m respectively. The buckling pressure for a given mode is obtained by multiplying the corresponding eigenvalue with the reference pressure. Figs. 9–11 show plan views of the first five modes for the spherical dome with $t_s = 0.7$ m, the paraboloid of revolution with $t_s = 1.5$ m, and the parabolic toroid with $t_s = 0.25$ m. All buckling modes are characterised by a relatively high number of waves in the circumferential direction, but only one in the meridional direction, except for the parabolic toroid which has three dimples in the meridional direction. It is also noted that the eigenvalues occur in identical pairs (repeated eigenvalues), with the

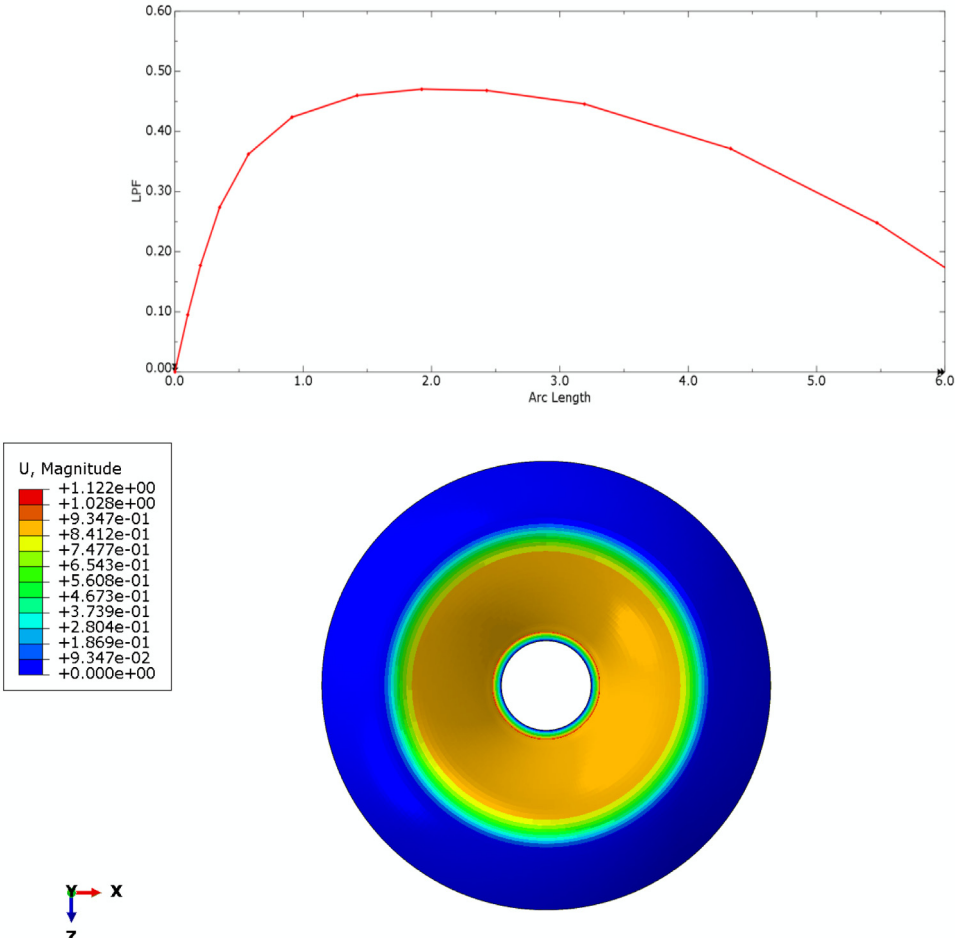

Fig. 25. Load factor (LPF) vs. arc-length for the parabolic toroid: Case 1: $t_s = 0.05$ m. The deformation image is taken at arc-length 5.469 and LPF 0.248.

values of the pairs being very close to each other. The phenomenon of repeated eigenvalues is characteristic of structural systems with symmetry, and is not limited to buckling; it is also encountered in vibration problems [44].

Figs. 12–14 show the first mode (which corresponds to the lowest buckling pressure) for various t_s values of the spherical dome, the paraboloid of revolution and the parabolic toroid. The eigenvalues and corresponding buckling pressures are plotted versus t_s in Fig. 15.

From these plots, we see that eigenvalues range from 6.09 to 62.04 in the case of the spherical dome, and 5.46 to 30.08 in the case of the paraboloid of revolution, which represent very high factors of safety against buckling. For example, an eigenvalue of 62.04 means that the liquid would have to be 62.04 times denser than water for buckling to occur! Of course, we have not accounted for imperfections here, but these high factors of safety for the perfect shells give us confidence that the shells are likely to be still quite safe even after accounting for imperfections. Imperfections will be taken into account in the section on nonlinear buckling.

For the parabolic toroid, the negative eigenvalues (ranging from −6.88 to −72.45) are an indication that buckling only occurs if the loading is reversed. Here, we have simply taken the lowest five values (whether positive or negative), and they happen to be all negative. In fact, as elaborated further in the next section, eigenvalues of the parabolic toroid all remain negative until we get to high mode numbers in excess of 100, when positive eigenvalues start to emerge.

Fig. 15 also reveals that as the parameter t_s is increased, the gain in buckling capacity of the shell becomes more rapid, a trend that is particularly noticeable in the case of the spherical dome.

7. Nonlinear buckling analysis

A finite element non-linear buckling analysis was done on three shell structures using a Riks solution algorithm within the programme ABAQUS [43]. As in the linear eigenvalue buckling analysis, fully integrated S4 general shell elements were used, to generate the same meshes as before (see Fig. 8). The edges of the shells were assumed to be fully restrained against translation and rotation. The main additional feature in the modelling of the shell geometry was the introduction of geometric imperfections. Imperfections may exist prior to the application of any loads as physical features of the real shell, or they may arise in the course of the loading as a result of the elastic bending deformations of the shell, or the elastic buckling modes. In this study, we will assume imperfections are related to the eigenmodes of linear buckling.

Now, in the absence of imperfections, shells normally exhibit a stiff load-deformation response until a point of bifurcation is reached, where the solution may branch along one of two or more possible paths, leading to numerical difficulties in the tracing of the postbuckling behaviour. One advantage of introducing imperfections is that we avoid this type of numerical difficulty, as the shell has a significant bending response right from the beginning, which causes the buckling to proceed along a more predictable path. The imperfections applied to each shell were taken to be a linear combination of the first ten modes as obtained from the eigenvalue buckling analysis:

$$\delta = \sum_{m=1}^{10} A_m \Delta u_m \tag{19}$$

where Δu_m and A_m are the normalised deflections and the amplitude of mode m, respectively. The amplitude of the linear buckling modes are

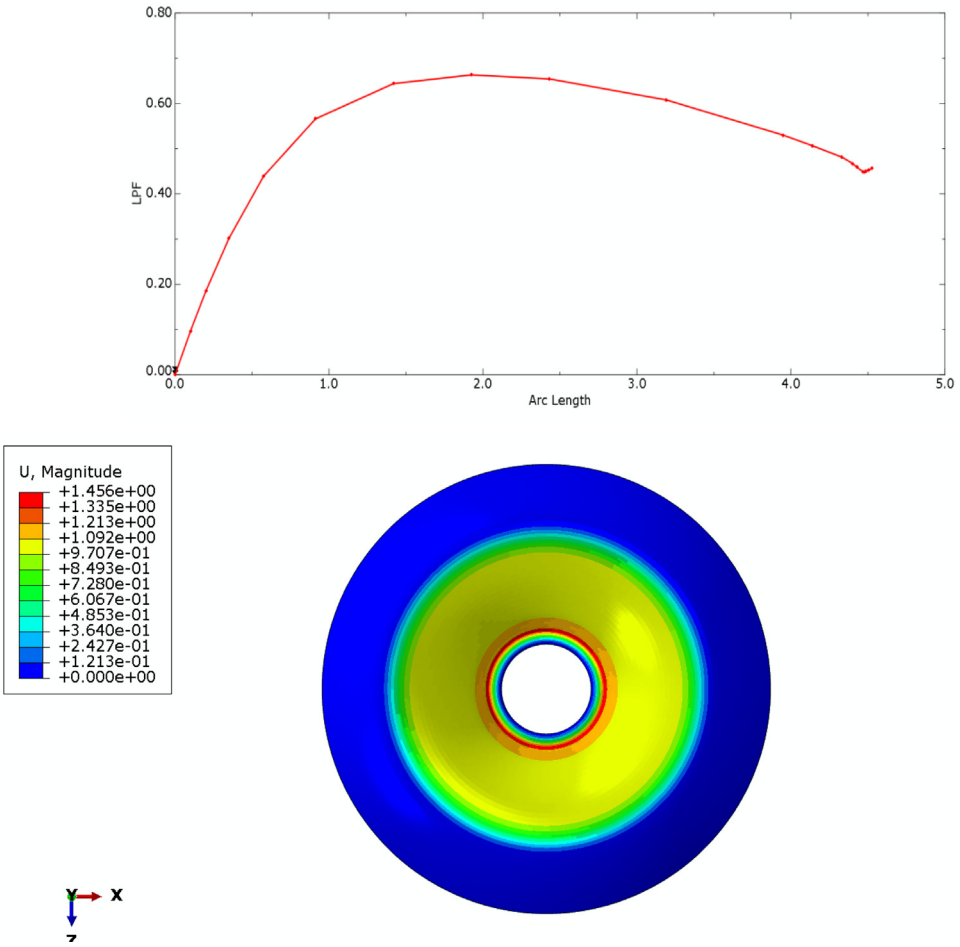

Fig. 26. Load factor (LPF) vs. arc-length for the parabolic toroid: Case 2: $t_s = 0.15$ m. The deformation image is taken at arc-length 4.401 and LPF 0.467.

calculated as follows:

$$A_1 = 0.1t_o \;;\; A_m = \frac{A_{m-1}}{2} \text{ for } m \geq 2 \tag{20}$$

where t_o is the shell thickness in the unthickened part of the dome. Thus, the amplitude of the first mode is taken as $0.1t_o$ (i.e. 10% of the minimum shell thickness), the amplitude of the 2nd mode as half of that of the 1st mode, the amplitude of the 3rd mode as half of that of the 2nd mode, and so on. With these assigned amplitudes, the first 10 linear buckling modes are then added together to give the required imperfection magnitude and shape. Note that the first linear buckling mode has the greatest weighting. This method of accounting for imperfections results in a combined imperfection amplitude that does not exceed $0.2t_o$ (i.e. 20% of the minimum shell thickness).

While a detailed imperfection-sensitivity analysis was not conducted, a comparison of the results of two arbitrary but different imperfection amplitudes showed that imperfection amplitude does have a significant influence on the buckling strength of the shell, a finding which is in keeping with the observations of other investigators [45]. However, the imperfections given by Eq. (20) are considered to be realistic enough for concrete shells which, being relatively thick, are not as vulnerable to manufacturing errors as steel shells. Moreover, the erection of formwork for doubly-curved concrete shells, and the placement of the wet concrete, are considered as very specialised tasks in the civil-engineering construction industry, and would be undertaken by highly-skilled workers under closely controlled conditions, which greatly reduces the chances of geometric imperfections larger than those considered here. In the unlikely event that the imperfections of the concrete shell are of an amplitude larger than $0.2t_o$ (20% of the minimum shell thickness), the conclusions drawn from the present nonlinear buckling analysis might not be valid.

The results for the peak buckling pressure as yielded by the nonlinear Riks analysis, for various t_s values of the spherical dome, the paraboloid of revolution and the parabolic toroid, are given in Tables 5 to 7. To facilitate comparison, the second last column shows the buckling pressure as calculated from the linear buckling analysis. The last column gives the ratio of nonlinear peak pressure to linear buckling pressure, denoted by ξ.

From Tables 5 to 7, it may be seen that the linear eigenvalue analysis overestimates the buckling pressure (in comparison with the Riks nonlinear analysis) by a factor ξ ranging from 1.66 to 2.04 in the case of the spherical shell, 1.03 to 1.48 in the case of the paraboloid of revolution, and 1.33 to 1.86 in the case of the parabolic toroid. For the shells of positive Gaussian curvature (spherical dome and paraboloid of revolution), ξ generally decreases as t_s (shell thickness at the support) is increased. For the shell of negative Gaussian curvature (parabolic toroid), the opposite happens: ξ increases as t_s is increased.

The very high values of buckling pressure associated with the parabolic toroid may be explained in terms of the linear eigenvalue analysis: the lowest 100 eigenvalues are all negative, and positive eigenvalues (which are relevant for the given direction of loading) only start to emerge at relatively high mode numbers, when eigenvalues are already very high in magnitude. In practical terms, and as confirmed by the nonlinear analysis, the toroidal dome of present proportions will never buckle under partial-depth external water pressure, and so is perfectly safe in this regard.

Plots of the load proportionality factor (LPF) versus arc-length, as well as images of the progression of vertical deformation, are shown in

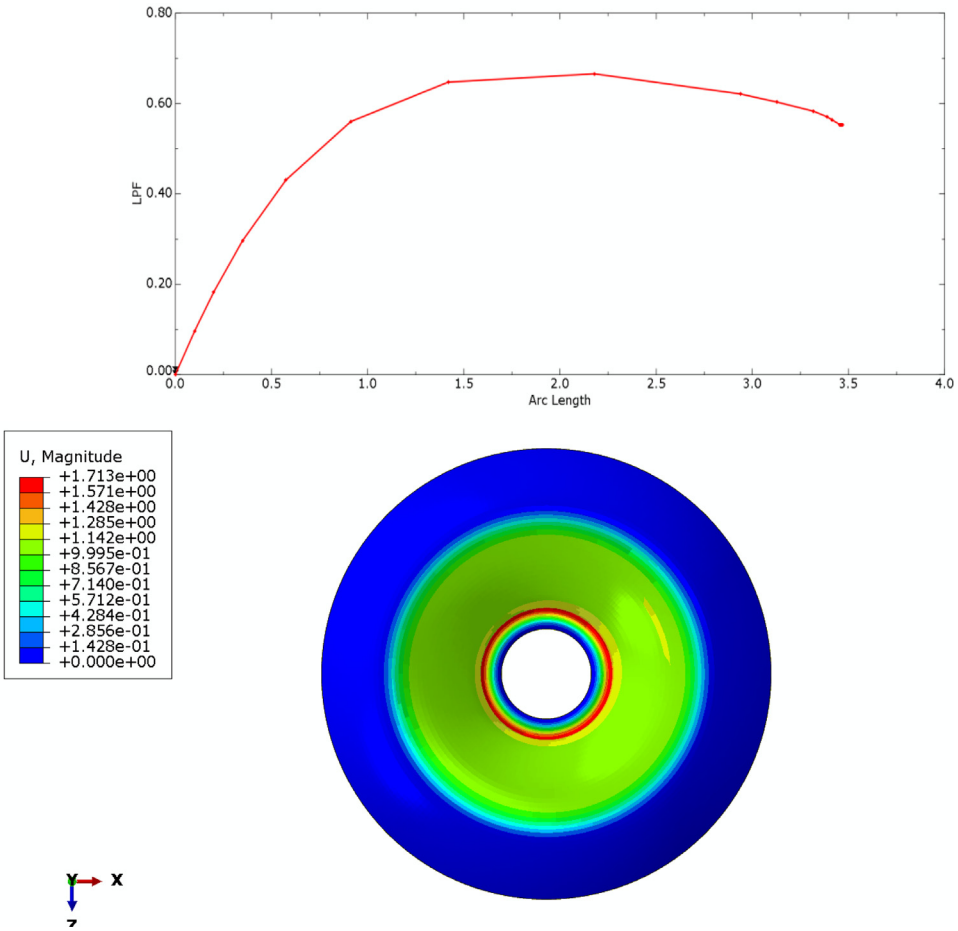

Fig. 27. Load factor (LPF) vs. arc-length for the parabolic toroid: Case 3: $t_s = 0.25$ m. The deformation image is taken at arc-length 3.458 and LPF 0.553.

Table 5
Buckling pressures for the spherical dome (h is in metres; $h_{max} = 8.038$ m).

Value of t_s ($t_o = 0.2$ m)	Reference pressure $\alpha\gamma h$ ($\gamma = 10{,}000$)	Riks peak load factor	Riks peak pressure (N/m^2) p_{rik}	Linear buckling pressure (N/m^2) p_{lin}	$\xi = \frac{p_{lin}}{p_{rik}}$
$t_s = 0.2$ m	50,000 h	0.597	29,850 h	60,900 h	2.04
$t_s = 0.3$ m	100,000 h	0.687	68,700 h	126,900 h	1.85
$t_s = 0.4$ m	200,000 h	0.605	121,000 h	216,400 h	1.79
$t_s = 0.5$ m	300,000 h	0.597	179,100 h	328,100 h	1.83
$t_s = 0.6$ m	400,000 h	0.645	258,000 h	462,300 h	1.79
$t_s = 0.7$ m	500,000 h	0.746	373,000 h	620,400 h	1.66

Table 6
Buckling pressures for the paraboloid of revolution (h is in metres; $h_{max} = 10.0$ m).

Value of t_s ($t_o = 0.1$ m)	Reference pressure $\alpha\gamma h$ ($\gamma = 10{,}000$)	Riks peak load factor	Riks peak pressure (N/m^2) p_{rik}	Linear buckling pressure (N/m^2) p_{lin}	$\xi = \frac{p_{lin}}{p_{rik}}$
$t_s = 0.5$ m	50,000 h	0.738	36,900 h	54,600 h	1.48
$t_s = 1.0$ m	300,000 h	0.431	129,300 h	164,700 h	1.27
$t_s = 1.5$ m	400,000 h	0.733	293,200 h	300,800 h	1.03

Table 7
Buckling pressures for the parabolic toroid (h is in metres; $h_{max} = 5.0$ m).

Value of t_s ($t_o = 0.05$ m)	Reference pressure $\alpha\gamma h$ ($\gamma = 10{,}000$)	Riks peak load factor	Riks peak pressure (N/m^2) p_{rik}	Linear buckling pressure (N/m^2) p_{lin}	$\xi = \frac{p_{lin}}{p_{rik}}$
$t_s = 0.05$ m	3 x 10^6 h	0.471	1,413,000 h	1,878,000 h	1.33
$t_s = 0.15$ m	10 x 10^6 h	0.663	6,630,000 h	10,543,000 h	1.59
$t_s = 0.25$ m	20 x 10^6 h	0.666	13,320,000 h	24,812,000 h	1.86

Figs. 16 to 27. For the spherical dome, the deformations of the shell are shown at four stages (with LPF value given): at a point before the peak load; (ii) at the peak load; (iii) at two points after the peak load. In all cases, the pattern of the imposed initial imperfections is evident at the early stage of buckling, but as the displacement progresses, the buckling dimples coalesce to one roughly-circular zone.

The three cases of the paraboloid of revolution display different behaviours. For the smallest value of shell thickness at the support

(t_s = 0.5 m), the postbuckling response is characterised by a continuous decline in load-carrying capacity leading to collapse. For the thicker shells (t_s = 1.0 m and t_s = 1.5 m), the postbuckling response remains generally flat (load-carrying capacity more or less constant) with increasing deformation, until at some stage there is a rapid decline in load-carrying capacity leading to collapse. Furthermore, the post-peak deformations do not coalesce to one single deformed region, as was observed in the case of the spherical dome.

The behaviour of the parabolic toroid is very different. The load-deformation response is smoothly continuous throughout, gradually maximising and then descending rather slowly. At the very high load levels at which buckling occurs, it seems large axisymmetric bending deformations dominate the behaviour of the shell just before that, and the axisymmetric pattern is preserved as the shell buckles, and maintained well into the postbuckling range, until the shell collapses. This is clearly evident in the images of Figs. 25 to 27. As already mentioned, this buckling behaviour has no significance, because the shell would have failed by material crushing or material rupture at load levels that are much lower than the buckling loads.

8. Concluding remarks

After discussing the potential merits of the concept of dual-purpose concrete domes, some possible configurations for both shelter/roofing and water storage/retention have been evaluated with regard to stress and buckling resistance. These configurations have included a spherical-conical roof assembly carrying water over the top, a paraboloidal hall retaining water around its lower circumference, and a toroidal hall retaining water in a central lake. While both self-weight and hydrostatic water pressure were taken into account in a previous study, the focus of the present work has been hydrostatic loading, which causes much more severe effects.

The first phase of the investigation on dual-purpose concrete domes comprised an analytical study based on the membrane theory of shells. This showed that hydrostatic water pressure induces relatively large stresses in the shells, but these can be effectively controlled through gradual thickening of the shell over the submerged region of the dome. The present study has extended the analytical work to the quantification of bending effects in the vicinity of the supported edge of the gradually-thickened dome, which the membrane theory cannot account for. Closed-form solutions for shell-edge redundants have been derived, and a numerical example (based on the spherical dome) considered. While a gradual increase of shell thickness over the lower region of the dome has the effect of extending the range of the bending disturbance, it also has the beneficial effect of significantly lowering the magnitude of the flexural stresses, and providing enough space for the placement of two layers of tensile reinforcement in the edge zone.

The previous study had also revealed a rapid increase in compressive membrane action as one moved along the shell meridian, from the surface of the water towards the base of the shell, which in turn was a clear indication of the high likehood of shell buckling. In the present study, both a linear eigenvalue buckling analysis, and a nonlinear analysis accounting for geometric imperfections, have been conducted using the finite-element method. It has been shown that gradual shell thickening is also effective in enhancing the buckling resistance of the shell.

Specifically, and as shown by the linear buckling analysis, as the t_s value (the eventual shell thickness at the support) is made larger in comparison with the t_o value (the initial shell thickness at the level of zero water pressure), the gain in buckling capacity of the shell becomes more rapid, a trend that is particularly noticeable in the case of the spherical dome. The high factors of safety observed for the synclastic domes (spherical and paraboloidal) give confidence that these dual-purpose shells are likely to retain a good margin of safety even after imperfections have been accounted for, a conclusion that has been confirmed by the results of the nonlinear analysis.

From the numerical examples that have been considered (these are representative of typical proportions for dual-purpose concrete domes), it has been shown that the linear eigenvalue analysis overestimates the buckling pressure (in comparison with the Riks nonlinear analysis) by a factor ξ ranging from 1.66 to 2.04 in the case of the spherical shell, 1.03 to 1.48 in the case of the paraboloid of revolution, and 1.33 to 1.86 in the case of the parabolic toroid. For the shells of positive Gaussian curvature (spherical dome and paraboloid of revolution), ξ generally decreases as t_s (shell thickness at the support) is increased. For the shell of negative Gaussian curvature (parabolic toroid), the opposite happens: ξ increases as t_s is increased.

While the nonlinear buckling pressures for both the spherical dome and the paraboloid of revolution are significantly higher (by factors ranging from 5 to 30) than the hydrostatic pressure under service conditions, this finding applies even more for the parabolic toroid, for which it has been shown that buckling under partial-depth external water pressure would never occur, at least in the range of proportions that have been studied. Thus, the anticlastic wall of a parabolic toroidal dome will not fail by buckling of the shell under the hydrostatic pressure of the water in the central reservoir. For the synclastic domes, once buckling has commenced, the load-carrying capacity of the shell progressively decreases with deformation, quickly leading to collapse. However, the precise postbuckling behaviour depends on the thickness proportions of the shell.

The overall conclusion is that the novel concept of dual-purpose concrete shells is viable from a structural point of view. It is hoped that this finding will provide added impetus for the revival of the use of elegant thin concrete shells for the roofing of public spaces once again.

CRediT authorship contribution statement

Alphose Zingoni: 100%. This is a sole-authored publication..

Declaration of competing interest

The authors declare that they have no known competing financial interests or personal relationships that could have appeared to influence the work reported in this paper.

Acknowledgements

The author wishes to thank the following individuals: Greg Mitchell (FEAS) and Kenny Mudenda (Univ. of Cape Town) for assistance with aspects of the finite-element modelling; Angus Rule (Univ. of Cape Town) for the drawings of Fig. 1; Nosa Enoma (Univ. of Benin) for the drawings of Fig. 2 and the plots of Figs. 3 to 5; Malefetsane Letsika (Univ. of Cape Town) for the plots of Figs. 7 and 15.

References

[1] P.B. Morice, H. Tottenham, The early development of reinforced concrete shells, Struct. Build. (Proc. Inst. Civ. Eng.) 116 (1996) 373–380.
[2] D. Veenendaal, M. West, P. Block, History and overview of fabric formwork: Using fabrics for concrete casting, Struct. Concr. 12 (2011) 164–177.
[3] W. Hawkins, J. Orr, T. Ibell, P. Shepherd, H. Michael, B. Kromoser, A. Michaelski, R. Pedreschi, H.R. Schipper, D. Veenendaal, R. Wansdronk, M. West, A. Pronk, Flexible formwork technologies: A state of the art review, Struct. Concr. 17 (2016) 911–935.
[4] R. Foster, T. Ibell, A numerical solution for the shape of fabric-formed concrete structures, Structures 8 (2016) 17–24.
[5] T. Tysmans, S. Adriaenssens, J. Wastiels, Form finding methodology for force-modelled anticlastic shells in glass fibre textile reinforced cement composites, Eng. Struct. 33 (2011) 2603–2611.
[6] S. Adriaenssens, P. Block, D. Veenendaal, C. Williams (Eds.), Shell Structures for Architecture: Form Finding and Optimisation, Routledge, 2014.
[7] A. Zingoni, N. Enoma, Dual-purpose concrete domes: a strategy for the revival of thin concrete shell roofs, Structures 28 (2020) 2686–2703.
[8] C.R. Calladine, The theory of shell structures: Aims and methods, Int. J. Mech. Sci. 24 (1982) 219–230.
[9] C.R. Calladine, Theory of Shell Structures, Cambridge University Press, 1983.

[10] P.L. Gould, Analysis of Shells and Plates, Springer-Verlag, 1988.
[11] V.V. Novozhilov, Thin Shell Theory, Wolters-Noordhoff Publishing, 1970.
[12] A. Zingoni, Shell Structures in Civil and Mechanical Engineering: Theory and Analysis, ICE Publishing (Institution of Civil Engineers), 2018.
[13] W. Flügge, Stresses in Shells, Springer, 1973.
[14] M.N. Pavlovic, A. Zingoni, On the elastic design of concrete domes, Struct. Eng. Rev. 6 (1994) 57–69.
[15] A. Zingoni, M.N. Pavlovic, Effect of support conditions in liquid-filled spherical vessels: Inclined supports, Proc. Inst. Civ. Eng. 2 91 (1991) 347–363.
[16] A. Zingoni, Discontinuity effects at cone-cone axisymmetric shell junctions, Thin-Walled Struct. 40 (2002) 877–891.
[17] S.N. Krivoshapko, Research on general and axisymmetric ellipsoidal shells used as domes, pressure vessels and tanks, Appl. Mech. Rev. (ASME) 60 (2007) 336–355.
[18] A. Zingoni, N. Enoma, N. Govender, Equatorial bending of an elliptic toroidal shell, Thin-Walled Struct. 96 (2015) 286–294.
[19] A. Zingoni, Stresses and deformations in egg-shaped sludge digesters: Discontinuity effects, Eng. Struct. 23 (2001) 1373–1382.
[20] A. Zingoni, B. Mokhothu, N. Enoma, A theoretical formulation for the stress analysis of multi-segmented spherical shells for high-volume liquid containment, Eng. Struct. 87 (2015) 21–31.
[21] A. Zingoni, N. Enoma, On the strength and stability of elliptic toroidal domes, Eng. Struct. 207 (2020) 110241.
[22] A. Zingoni, Self-weight stresses in hyperbolic cooling towers of general shape, Int. J. Space Struct. 14 (1999) 281–294.
[23] A. Zingoni, On membrane solutions for elevated shell-of-revolution tanks of certain meridional profiles, Thin-Walled Struct. 22 (1995) 121–142.
[24] A. Zingoni, Parametric stress distribution in shell-of-revolution sludge digesters of parabolic ogival form, Thin-Walled Struct. 40 (2002) 691–702.
[25] A. Zingoni, Liquid-containment shells of revolution: A review of recent studies on strength, stability and dynamics, Thin-Walled Struct. 87 (2015) 102–114.
[26] L.A. Godoy, Buckling of vertical oil storage steel tanks: Review of static buckling studies, Thin-Walled Struct. 103 (2016) 1–21.
[27] E. Hamed, M.A. Bradford, R.I. Gilbert, Nonlinear long-term behaviour of spherical shallow thin-walled concrete shells of revolution, Int. J. Solids Struct. 47 (2) (2010) 204–215.
[28] M. Sato, M.A. Wadee, K. Iiboshi, T. Sekizawa, H. Shima, Buckling patterns of complete spherical shells filled with an elastic medium under external pressure, Int. J. Mech. Sci. 59 (1) (2012) 22–30.
[29] M. Imran, D. Shi, L. Tong, A. Elahi, M. Uddin, On the elastic buckling of cross-ply composite closed cylindrical shell under hydrostatic pressure, Ocean Eng. 227 (2021) 108633.
[30] A. Zingoni, N. Enoma, Strength and stability of spherical-conical shell assemblies under external hydrostatic pressure, Thin-Walled Struct. 146 (2020) 106472.
[31] L.H. Sobel, W. Flügge, Stability of toroidal shells under uniform external pressure, Am. Inst. Aeronaut. Astronaut. (AIAA) J. 5 (1967) 425–431.
[32] P.F. Jordan, Buckling of toroidal shells under hydrostatic pressure, Am. Inst. Aeronaut. Astronaut. (AIAA) J. 11 (10) (1973) 1439–1441.
[33] W. Jiammeepreecha, S. Chucheepsakul, Nonlinear static analysis of an underwater elastic semi-toroidal shell, Thin-Walled Struct. 116 (2017) 12–18.
[34] N. Enoma, A. Zingoni, Buckling of an externally pressurised toroidal shell of revolution with a doubly-symmetric parabolic-ogival cross-section, Int. J. Press. Vessels Pip. 183 (2020) 104106.
[35] E.M. Sosa, L.A. Godoy, Challenges in the computation of lower-bound buckling loads for tanks under wind pressures, Thin-Walled Struct. 48 (12) (2010) 935–945.
[36] C.A. Burgos, R.C. Jaca, J.L. Lassig, L.A. Godoy, Wind buckling of tanks with conical roof considering shielding by another tank, Thin-Walled Struct. 84 (2014) 226–240.
[37] P. Jasion, K. Magnucki, Elastic buckling of clothoidal-spherical shells under external pressure: Theoretical study, Thin-Walled Struct. 86 (2015) 18–23.
[38] P. Jasion, K. Magnucki, Theoretical investigation of the strength and stability of special pseudospherical shells under external pressure, Thin-Walled Struct. 93 (2015) 88–93.
[39] S. Wang, V. Notario, M. Garlock, B. Glisic, Parameterization of hydrostatic behavior of deployable hypar umbrellas as flood barriers, Thin-Walled Struct. 163 (2021) 107650.
[40] S. Wang, M. Garlock, B. Glisic, Hydrostatic response of deployable hyperbolic-paraboloid umbrellas as coastal armor, J. Struct. Eng. 146 (6) (2020) 04020096.
[41] A. Zingoni, M.N. Pavlovic, Computation of bending disturbances in axisymmetrically loaded spherical shells: A study of the accuracy of Geckeler's approximation, Eng. Comput. 7 (2) (1990) 125–143.
[42] A. Zingoni, M.N. Pavlovic, On edge-disturbance interaction and decoupling errors in thin-walled nonshallow spherical-shell frusta, Thin-Walled Struct. 13 (1992) 375–386.
[43] ABAQUS Standard, Hibbit, Karlsson and Sorenson Inc, Newark (California), 1998.
[44] A. Zingoni, A group-theoretic finite-difference formulation for plate eigenvalue problems, Comput. Struct. 112/113 (2012) 266–282.
[45] H.N.R. Wagner, C. Hühne, J. Zhang, W. Tang, On the imperfection sensitivity and design of spherical domes under external pressure, Int. J. Press. Vessels Pip. 179 (2020) 104015.